Available online at www.sciencedirect.com

ScienceDirect

journal homepage: www.elsevier.com/locate/he

Numerical modelling of a heavy-duty diesel-hydrogen dual-fuel engine with late high pressure hydrogen direct injection and diesel pilot

C.J. Ramsay, K.K.J. Ranga Dinesh *

Energy Technology Research Group, School of Engineering, Faculty of Engineering and Physical Sciences, University of Southampton, SO17 1BJ, Southampton, UK

HIGHLIGHTS

- Combustion performance of a diesel-hydrogen dual direct injection engine is investigated.
- Four distinct phases of combustion are identified.
- Very high hydrogen energy share works well at high load.
- Very high hydrogen energy share requires improvement at low load.

GRAPHICAL ABSTRACT

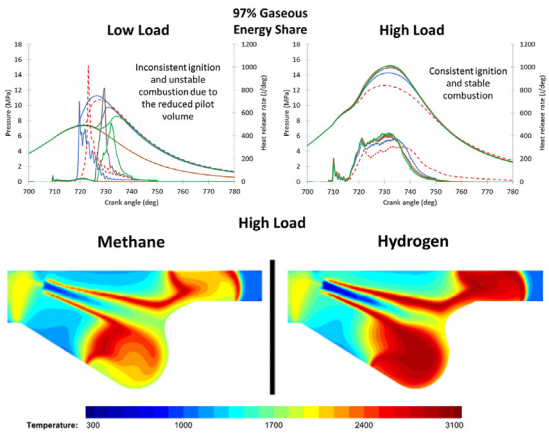

ARTICLE INFO

Article history:
Received 29 June 2023
Received in revised form
18 August 2023
Accepted 2 September 2023
Available online xxx

Keywords:
Hydrogen direct injection
Diesel pilot injection
Dual direct injection
Dual-fuel engine

ABSTRACT

Direct gaseous fuel injection in internal combustion engines is a potential strategy for improving in-cylinder combustion processes and performance while reducing emissions and increasing hydrogen energy share (HES). Through use of numerical modelling, the current study explores combustion in a compression ignition engine utilising a late compression/early power stroke direct gaseous hydrogen injection ignited by a diesel pilot at up to 99% HES. The combustion process of hydrogen in this type of engine is mapped out and compared to that of the same engine using methane direct injection. Four distinct phases of combustion are found which differ from that of pure diesel operation. Interaction of the injected gas jet with the chamber walls is found to have a considerable impact on performance and emission characteristics and is a factor which needs to be explored in greater detail in future studies. Considerable performance increase and carbon-based emission reductions are identified at up to 99% HES at high load but low load

* *Corresponding author.*
E-mail address: dinesh.kahanda-koralage@soton.ac.uk (K.K.J.R. Dinesh).
https://doi.org/10.1016/j.ijhydene.2023.09.019

Performance and emissions
Modelling and simulation

performance greatly deteriorated when 95% HES was exceeded due to a much reduced diesel pilot struggling to ignite the main hydrogen injection.

1. Introduction

Renewable energy has been thrust into the spotlight in recent years due to rising global awareness of the environmental impacts of fossil fuel combustion in conjunction with growing energy demands [1]. Hydrogen (H_2) has a promising future as both a clean energy carrier and fuel source but first a number of factors such as production, transport, storage and utilisation must be addressed before it can be adopted.

This study focuses on utilisation in vehicles, in which there are two main potential avenues, namely hydrogen fuel cells and hydrogen powered internal combustion engines (ICEs). Significant research and development has been carried out on hydrogen fuel cells where electrochemical reactions of hydrogen and an oxidiser are used to produce electricity which is then used to power the vehicle [2]. While fuel cell vehicles are likely the future in terms of near-zero emissions, production costs are prohibitive while also requiring very high purity hydrogen to prevent system degradation [3] and thus a bridging technology which can help improve infrastructure and drive down costs is required [4]. ICEs have the potential to achieve this goal as conversion of a conventional spark ignition (SI) or compression ignition (CI) engine to being fuelled by a gas such as hydrogen is relatively straightforwards and thus costs a fraction of a fuel cell vehicles current price of production while also not requiring as high a purity fuel [5]. Therefore, if hydrogen fuelled ICEs were to become an attractive option in terms of performance, emissions and price comparative to conventional ICEs, then any infrastructure developed would also facilitate an eventual transition to fuel cell vehicles.

Currently, CI engines fuelled by diesel play a vital role in many heavy-duty transport, power generation, agricultural and industrial applications due to the various benefits of CI engine combustion and its operating cycle. These benefits include superior torque, greater power output, higher thermal efficiency, better fuel economy and reliability when compared with SI engines [6]. Unfortunately however, diesel engines generally emit higher levels of harmful pollutant emissions such as nitric oxides (NO_x), unburned hydrocarbons (UHC), carbon monoxide (CO) and soot. Utilisation of hydrogen in heavy-duty CI engines can lead to a reduction in carbon-based emissions while maintaining or even improving performance [7,8]. However, efficient utilisation is not a trivial task and thus improvements and optimisation of the various strategies used for hydrogen combustion in CI engines is required.

Generally utilisation of hydrogen in CI engines will require operation in a dual-fuel mode where a more reactive fuel such as diesel is used as a pilot fuel to ignite the high autoigniton temperature hydrogen fuel. The inherent complexity of dual-fuel engine design and operation in terms of both engine fuelling and combustion modes means that both experimental and numerical investigation is required to gain insights on the various physical phenomena which occur such as the flow induced by fuel injection, ignition, flame propagation, heat release and formation of pollutant emissions.

Gaining insight into the processes occurring during dual direct injection diesel-hydrogen CI engine operation is essential for the advancement of heavy-duty hydrogen internal combustion engine technology. High pressure direct injection (HPDI) of the gaseous fuel close to top dead centre (TDC) aiming for non-premixed combustion should allow for greater power output and higher hydrogen substitution rates across all load conditions when compared to either early compression stroke direct injection or intake induction operation [8,9]. Fig. 1 illustrates the general combustion process present in a late hydrogen HPDI engine utilising a diesel pilot as an ignition source for the injected hydrogen jet. Unlike premixed operation, late HPDI of hydrogen completely avoids any potential pre-ignition or backfire so the likes of load and compression ratio do not need to be lowered allowing for maximum power output, which is especially important for heavy-duty applications. Another benefit is the potential for higher hydrogen substitution rates across all load conditions as the diesel pilot volume can be reduced because it's much easier to ignite the incoming hydrogen jet than the lean homogeneous mixtures used in premixed operation. Currently investigations into late compression/early power stroke hydrogen HPDI with diesel pilot ignition are scarce and further experimental and modelling studies are required to assess the impacts of the strategy on engine combustion, performance and emissions outputs.

The majority of the hydrogen HPDI investigations in the literature have been in SI [10–14], glow plug [15–18] or HCCI [8,19–22] type engines so there lies many unknowns with regards to utilisation in dual-fuel CI engines aiming for a non-premixed mode of combustion [8]. Hydrogen HPDI aiming for non-premixed combustion modes have only recently begun to gain traction. Rottengruber et al. [23] aimed for non-premixed combustion similar to diesel operation and investigated pure hydrogen direct injection in a compression ignition engine, however, inlet pre-heating to 343 K was required to allow for reasonable autoignition delay timings which led to a reduction in performance. Similarly, Gomes Antunes et al. [24] also investigated a pure hydrogen direct injection CI engine and required pre-heating to 353 K for reasonable ignition delay. While this mode of operation may be reasonable the required high in-cylinder temperatures and reduction to intake air density are likely to both increase NO_x emissions and reduce performance.

Please cite this article as: Ramsay CJ, Dinesh KKJR, Numerical modelling of a heavy-duty diesel-hydrogen dual-fuel engine with late high pressure hydrogen direct injection and diesel pilot, International Journal of Hydrogen Energy, https://doi.org/10.1016/j.ijhydene.2023.09.019

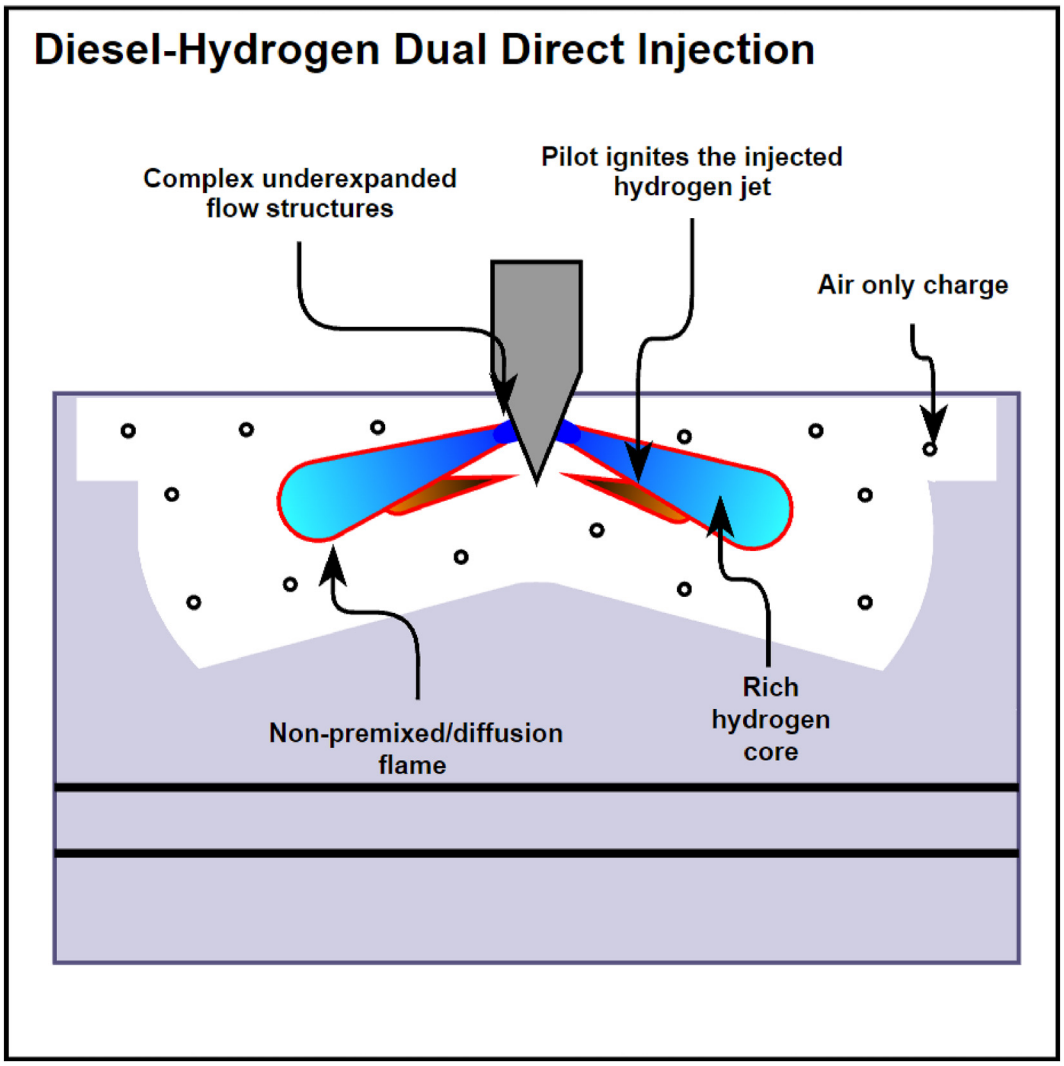

Fig. 1 – Example schematic of the combustion process in a late high pressure dual direct injection hydrogen-diesel dual-fuel engine.

With regard to dual-fuel engines, only a handful of studies were found in the literature directly addressing pilot ignited non-premixed hydrogen direct injection operation which are recent CFD studies carried out by Babayev et al. [25–27], Frankl et al. [28], Munshi et al. [9] and Liu et al. [29] as well as experimental studies by Liu et al. [30] and Rorimpandey et al. [31]. Babayev et al. [25, 26] have published a number of studies and validated a CFD model, comparing the combustion characteristics of a pure diesel CI engine to that of a pure hydrogen direct injection CI engine utilising a hydrogen pilot and hydrogen main injection. Distinct combustion phases were found which differ somewhat from the standard diesel combustion process. An optimisation study was also performed [27] which noted optimisation of the likes of piston bowl design and injection parameters such that more combustion occurs before the gas jet contacts the chamber walls can lead to improved combustion quality. Frankl et al. [28] also validated a CFD model and compared the combustion process of diesel pilot ignited direct hydrogen injection with direct ammonia injection. Again a similar combustion process with minimal premixing and a non-premixed flame surrounding the rich hydrogen core is noted, however, less jet-jet interaction is observed due to what appears to be a much shorter injection event and flat/square piston bowl which doesn't allow for the same type of movement of the jet along the walls as was observed in the engine studied by Babayev et al. [25]. Frankl et al. also found that the gaseous jet caused increased convection of the pilot combustion products into the piston bowl area. Munshi et al. [9] performed a numerical analysis which compared pure diesel operation to hydrogen intake induction, early cycle direct hydrogen injection and late compression/early power stroke hydrogen HPDI all operating with a diesel pilot. It was found that HPDI engine torque and efficiency was equal to or exceeded diesel operation and far exceeded possible torque and efficiency of the two premixed hydrogen cases while not suffering from knocking or unstable combustion. Liu et al. [29] carried out a CFD study which compared diesel pilot ignited late hydrogen HPDI to three types of premixed hydrogen combustion, namely port-fuelled SI, port-fuelled diesel pilot ignited and port-fuelled pre-chamber ignited. It was found that

Please cite this article as: Ramsay CJ, Dinesh KKJR, Numerical modelling of a heavy-duty diesel-hydrogen dual-fuel engine with late high pressure hydrogen direct injection and diesel pilot, International Journal of Hydrogen Energy, https://doi.org/10.1016/j.ijhydene.2023.09.019

the HPDI case could run at much higher compression ratios than the other types of operation which allowed for high thermal efficiency and power output. However, owing to the high temperatures of the diffusion flame at the jets periphery high NO_x levels and wall heat losses were also found, especially in comparison to the pre-chamber and SI engines as they could run at ultra-lean conditions where chamber temperatures remain low throughout. Liu et al. [30] carried out an experimental study on a compression ignition engine utilising HPDI of hydrogen with a diesel pilot at varying hydrogen energy shares (0–90%) and compared start of injection timings (180-0°CA before TDC). Primarily mixing controlled combustion was observed for SOI timings later than 20°CA before TDC, with lower peak in-cylinder pressures when compared to the earlier SOI cases which exhibited much higher levels of premixed combustion. The late HPDI cases generally led to lower NO_x emissions but also lower power outputs which was mostly due to the later combustion phasing in comparison to the premixed cases. Rorimpandey et al. [31] investigated the combustion process of pilot ignited hydrogen HPDI in an optical constant volume combustion chamber. They found that hydrogen ignition is delayed when the dwell time between pilot and main hydrogen injection is increased as the pilot combustion products begin to cool before the hydrogen is injected. Similar hydrogen ignition delay increases were also observed when ambient temperatures were lowered. In addition, they found that cycle-cycle variability increased greatly if the pilot fuel ignition occurred towards the end of or after the hydrogen injection, leading to inconsistent heat release rates and flame evolution.

To this authors knowledge no other CFD or experimental studies on this form of hydrogen CI engine combustion are present in the literature, and thus further investigations are required. For the most part pilot ignited non-premixed HPDI studies have utilised methane/natural gas rather than hydrogen with the likes of injection pressure [32,33], relative angle between injections [34], nozzle diameter [35,35,36], relative injection timings/strategies [35–39], etc. all being investigated. However, due to hydrogen's disparate fuel properties conclusions cannot be drawn from the studies on methane/natural-gas. Table 1 compares said properties to methane and various other fuels.

This study aims to map out the general combustion process of diesel pilot ignited late compression/early power stroke direct hydrogen injection CI engine operation while also identifying the benefits of late hydrogen HPDI and areas in which the combustion process can be optimised. Furthermore, comparisons are made between hydrogen and methane as the two gaseous fuels are both suitable candidates for emissions reductions in CI engines.

2. Numerical methodology and modelling setup

Three-dimensional unsteady Reynolds averaged Navier-Stokes (URANS) CFD simulations were performed using ANSYS Fluent 19.1 on the University of Southampton high performance computing cluster IRIDIS 4.

2.1. Governing equations

Simulations were carried out by solving compressible URANS equations for mass, momentum, energy and $N-1$ species transport equations, where N is the total number of species for a chemically reacting mixture using finite volume method.

Mass:

$$\frac{\partial \rho}{\partial t}+\frac{\partial \rho \overline{u}_j}{\partial x_j}=S_m, \tag{1}$$

Momentum:

$$\frac{\partial \rho \overline{u}_i}{\partial t}+\frac{\partial \rho \overline{u_i} \overline{u_j}}{\partial x_j}=-\frac{\partial \overline{P}}{\partial x_i}+\frac{\partial}{\partial x_j}\left(\mu\left(\frac{\partial \overline{u}_j}{\partial x_i}+\frac{\partial \overline{u}_i}{\partial x_j}-\frac{2}{3}\delta_{ij}\frac{\partial \overline{u}_k}{\partial x_k}\right)\right)-\frac{\partial \rho \overline{u_i' u_j'}}{\partial x_j}+S_i. \tag{2}$$

Energy:

$$\frac{\partial \rho \overline{H}}{\partial t}+\frac{\partial \rho \overline{u}_j \overline{H}}{\partial x_j}=\frac{\partial}{\partial x_j}\left(\frac{k_{eff}}{C_p}\frac{\partial \overline{H}}{\partial x_j}\right)+S_h, \tag{3}$$

Species:

$$\frac{\partial \rho \overline{Y}_n}{\partial t}+\frac{\partial \rho \overline{u}_i \overline{Y}_n}{\partial x_j}=-\frac{\partial J_n}{\partial x_j}+R_n+S_n \tag{4}$$

Table 1 – Properties of hydrogen, methane, gasoline, diesel, n-heptane and ammonia [6, 40–47] (diesel and gasoline are generally blended fuels so properties will vary from those listed).

Properties	Hydrogen	Methane	Gasoline	Diesel	n-Heptane	Ammonia
Chemical formula	H_2	CH_4	C_nH_2n	C_nH_{2n}	nC_7H_{16}	NH_3
Molecular weight (g/mol)	2.016	16.043	107	170	100.16	17.031
Density(kg/m^3)	0.08	0.65	750	840	692	0.73
Mass diffusivity in air (cm^2/s)	0.61	0.16	–	–	–	0.23
Flammability limits in air (vol%)	4–75	5–15	1–7.6	0.7–7.5	1.05–6.7	15–28
Burning velocity (m/s)	2.65–3.25	0.37–0.43	0.45	0.3	0.2–0.6	0.07
Quenching distance (mm)	0.61	2.00	2.00	–	–	8.95
Autoignition temperature (K)	858	813	523	483	479	930
Minimum ignition energy (mJ)	0.02	0.28	0.24	0.24	0.24	8
Adiabatic flame temperature (K)	2390	2226	2275	2275	2275	2080
Stoichiometric air/fuel ratio by mass	34.3	17.2	14.5	14.5	15.1	6.1
Lower heating value (MJ/kg)	120	50	43.4	42.6	44.6	18.6

Please cite this article as: Ramsay CJ, Dinesh KKJR, Numerical modelling of a heavy-duty diesel-hydrogen dual-fuel engine with late high pressure hydrogen direct injection and diesel pilot, International Journal of Hydrogen Energy, https://doi.org/10.1016/j.ijhydene.2023.09.019

Three further transport equations for pollutant emissions are solved post-time step for computational efficiency. NO_x emissions are calculated using the following transport equation for the NO_x mass fraction, $\overline{Y}_{NO_x}$, accounting for thermal [48] and prompt [49] mechanisms

$$\frac{\partial \rho \overline{Y}_{NO_x}}{\partial t} + \frac{\partial \rho \overline{u}_j \overline{Y}_{NO_x}}{\partial x_j} = \frac{\partial}{\partial x_j}\left(\rho D \frac{\partial \overline{Y}_{NO_x}}{\partial x_j}\right) + S_{NO_x} \quad (5)$$

Soot emissions are calculated using the Moss-Brookes soot model [50] using acetylene as the inception species. Two additional transport equation are solved for the soot mass fraction, $\overline{Y}_{soot}$, given by

$$\frac{\partial \rho \overline{Y}_{soot}}{\partial t} + \frac{\partial \rho \overline{u}_j \overline{Y}_{soot}}{\partial x_j} = \frac{\partial}{\partial x_j}\left(\frac{\mu_t}{\sigma_{soot}} \frac{\partial \overline{Y}_{soot}}{\partial x_j}\right) + \frac{dM}{dt} \quad (6)$$

and the normalised radical nuclei concentration $\overline{b^*}_{nuc}$

$$\frac{\partial \rho \overline{b^*}_{nuc}}{\partial t} + \frac{\partial \rho \overline{u}_j \overline{b^*}_{nuc}}{\partial x_j} = \frac{\partial}{\partial x_j}\left(\frac{\mu_t}{\sigma_{nuc}} \frac{\partial \overline{b^*}_{nuc}}{\partial x_j}\right) + \frac{1}{N^*_{norm}} \frac{dN^*}{dt}, \quad (7)$$

where ρ is the density of the fluid, t is time, $\overline{u}_j$ a component of the mean velocity vector, u'_j a component of the fluctuating velocity vector, x_j a component of the position vector, S_m the source term accounting for mass added by fuel spray, P is pressure, μ is molecular viscosity, S_i a component of the body forces, d_{ij} the Kronecker delta, $\overline{H}$ the mean total enthalpy, k_{eff} the effective conductivity, C_p the specific heat capacity of the fluid, S_h the source term accounting for any further heat losses, $\overline{Y}_n$ is the mass fraction of species n, J_n is the diffusion flux of the given species, R_n the net rate of production of the given species by chemical reaction, S_n the rate of creation of the species by the discrete phase injection and any other sources, D is the effective diffusion coefficient, S_{NO} is the source term for any other NO_x production due to thermal or prompt mechanisms, μ_t is the turbulent viscosity, σ_{soot} is the turbulent Prandtl number for soot transport, M is the soot mass concentration, σ_{nuc} is the turbulent Prandtl number for radical nuclei transport, N^* is the soot particle number density and N^*_{norm} is 10^{15} particles.

2.2. Numerical models and methods

Gaseous injections are dealt with using a modified gaseous sphere injection (GSI) model [51,52] which is implemented through use of user-defined functions (UDFs) which modify Fluent's Lagrangian discrete phase model (DPM). The GSI model is a computationally efficient method for simulating gaseous direct injection and further details of the model development and implementation can be found in [51]. Diesel injection is also handled by the DPM employing KHRT primary and secondary breakup [53], stochastic collision [54], dynamic-drag [55] and an impingement/splashing wall-film model [56,57]. In both types of injection, the DPM analytically tracks the injected droplets, grouped into parcels, with the fluid flow time step and models their coupled interactions with the continuous phase. The discrete random walk (DRW) stochastic tracking model [58] is used to predict turbulent dispersion of the particles. Realizable k-ϵ model [59] with standard wall functions is employed to model turbulent flow characteristics due to the models improvements over the standard k-ϵ model with regards to the round-jet anomaly [59]. Two additional transport equations for turbulent kinetic energy, k, and turbulent dissipation rate, ϵ, are solved. Combustion is modelled through use of the finite rate combustion model, with an adequately fine mesh such that the majority of the RANS scales are resolved, which couples the flow and chemical kinetics. The Chemkin-CFD solver along with Fluent's in situ adaptive tabulation (ISAT) algorithm [60] is employed to integrate reaction rates. The reduced Chalmers n-heptane mechanism [61] is supplemented with the GRI mech 3.0 [62] and a detailed hydrogen mechanism [63] to represent diesel, natural gas and hydrogen fuel chemistry leading to a chemical mechanism containing 48 species and 273 reactions. The nitrogen mechanism was removed from the GRI mech to reduce computational time and instead pollutant emissions are modelled post-process at the end of each time step. The Moss-Brookes soot model [50] is used to predict soot emissions and thermal and prompt NO_x development are accounted for to predict NO_x emissions. Dynamic mesh layering and smoothing is used to simulate the piston movement and keygrids are utilised which allow for a coarse mesh to be used during initial compression and a fine mesh during injection and combustion. Table 2 summarises the numerical models used.

A 3-D double precision analysis is carried out using Fluent's pressure based solver. The PISO pressure-velocity coupling algorithm is used to reformat the continuity equation and obtain a pressure field. Second order upwind schemes are used for the spatial discretisation. Least squares cell-based method is used to compute gradients. First-order implicit time-stepping is employed due to the variable time step profiles used in the simulations during fuel injection and combustion. Convergence criteria are set to converge at residuals of 10^{-3} apart from energy and post-processed scalars which are set to 10^{-6}. In all cases injected mass is also monitored to ensure the correct intended mass is delivered. Max iterations per time step are set to 50 with up to 10 post-time step iterations for the pollutant calculations. Table 3 outlines a summary of numerical discretisation methods employed during calculations.

2.3. Model validation

The engine model is based on an experimental study carried out by Faghani [39] for a dual direct injection diesel-natural gas engine and the parameters are summarised in Table 4. As there are 7 evenly spaced diesel and gas injectors in the engine a sector geometry representing 1/7th of the combustion chamber is created in ANSYS SpaceClaim and meshed using ANSYS meshing, Fig. 2. The sector contains one gas and one diesel injector both with an included spray angle of 140° and an interlace angle of 0°. Gaseous injection pressure is set at 25 MPa and diesel injection pressure at 27 MPa. Periodic boundary conditions are set at the side faces of the sector and constant temperature boundary conditions of 600 K and 650 K are set at the sector top face and piston bowl walls

Please cite this article as: Ramsay CJ, Dinesh KKJR, Numerical modelling of a heavy-duty diesel-hydrogen dual-fuel engine with late high pressure hydrogen direct injection and diesel pilot, International Journal of Hydrogen Energy, https://doi.org/10.1016/j.ijhydene.2023.09.019

Table 2 – Summary of the numerical models employed during the simulations.

Description	Model	
Viscous	Realizable k-ϵ	
Energy/Species	Species transport finite-rate combustion	
	Chemkin CFD solver with ISAT	
	Fuel oxidation mechanism representing n-heptane [61], methane [62] and hydrogen [63]	
NO_x	Thermal and prompt	
Soot	Moss-Brookes	
Dynamic mesh	Smoothing and layering	
Discrete Phase	GSI	Liquid
	Droplet particle	Droplet particle
	No breakup	KHRT primary & secondary breakup
	No collision	Stochastic collision
	Constant high Re spherical drag	Dynamic drag
	DRW turbulent dispersion	DRW turbulent dispersion
	Wall-reflection	Wall-film
	Laws: density-drag adjustment, core length transition	Laws: inert heating, vapourisation, boiling

Table 3 – Summary of numerical methods employed during simulations.

Description	Parameter	Method/model/value
Software	ANSYS Fluent 19.1	Finite volume method
Solver	General	Pressure-based
Pressure-velocity coupling	Flux type	Rhie-Chow
	Scheme	PISO
Spatial discretisation	Gradient	Least squares cell based
	Density	Second order upwind
	Momentum	Second order upwind
	Energy	Second order upwind
	k	Second order upwind
	ϵ	Second order upwind
	Species (N-1 equations)	Second order upwind
	Pollutant NO_x	Second order upwind
	Pollutant soot mass	Second order upwind
	Pollutant soot nuclei	Second order upwind
Temporal discretisation	Time	First order implicit

respectively and 500 K at the remainder of the chamber walls. Exhaust gas recirculation (EGR) level is adjusted by varying the initial charge composition, temperature and pressure using values measured in the experimental reference. Simulations are run from inlet valve close (IVC) to exhaust valve open (EVO) and layering is used to compute piston motion during the compression and expansion strokes. Results are then compared to the experimental measurements. Throughout this analysis the convention that 720°CA is TDC of the compression stroke is followed.

Table 4 – Summary of engine parameters based on experimental study by Faghani [39].

Engine Parameters	Value
Bore x stroke (mm)	137 x 169
Connecting rod (mm)	262
Swirl ratio	1.5
Compression ratio	17
Engine speed (RPM)	1500
IVC-EVO (CA)	630°–860°
Number of pilot injectors	7
Number of gas injectors	7
Pilot start of injection (CA)	703°
Gas start of injection (CA)	712°

A mesh sensitivity study is carried out using 4 different grid resolutions; coarse, medium, fine and very fine with maximum cell sizes of 1 mm, 0.4 mm, 0.35 mm and 0.3 mm respectively, see Table 5. To allow for reasonable computation times keygrids are used in all but the coarse mesh simulation. In the medium, fine and very fine cases the coarse grid is used from IVC to 700°CA (3° before pilot injection starts) before being replaced by a finer mesh, Fig. 2. This fine mesh is then used throughout both injections and the power stroke until EVO with a variable layering height which begins to coarsen after injections have finished. A variable time step size is used with 0.25°CA steps from IVC to 702°CA followed by 0.025°CA steps until 755°CA then 0.25°CA again until EVO.

As can be seen in Fig. 3 all grids apart from the most coarse predict in-cylinder pressure and heat release fairly well for the 18% EGR test case. The coarse grid predicts a slightly later ignition of the methane injection compared to the other grids and generally underpredicts the rate of combustion until around the time that the gaseous injection finishes, leading to a lower pressure than desired. Only small variation between the medium and fine grid is observed. The variation is largely

Please cite this article as: Ramsay CJ, Dinesh KKJR, Numerical modelling of a heavy-duty diesel-hydrogen dual-fuel engine with late high pressure hydrogen direct injection and diesel pilot, International Journal of Hydrogen Energy, https://doi.org/10.1016/j.ijhydene.2023.09.019

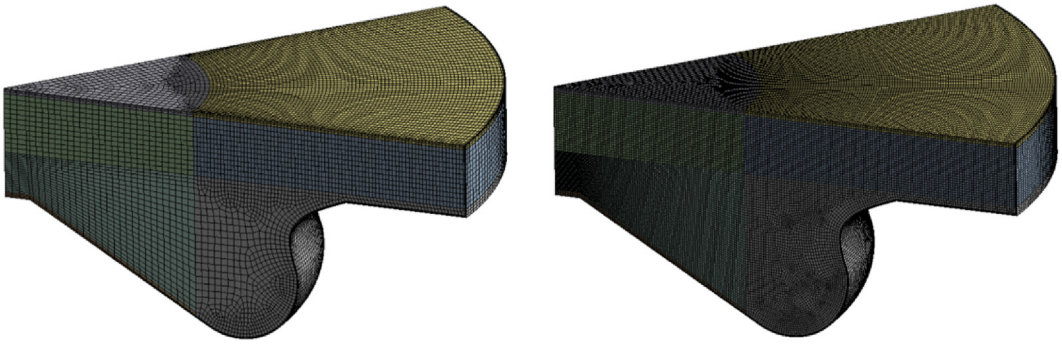

Fig. 2 – Sector mesh at 700°CA used in combustion simulations. Left shows the "coarse" grid used to compute the compression stroke prior to injection and right shows the "fine" keygrid, with a maximum mesh size of 0.35 mm, used during injection and combustion.

Table 5 – Mesh densities for the mesh independence study.

Mesh	Cell count at TDC	Max cell size (mm)	Run time
Coarse	50k	1	≈7h
Medium	300k	0.4	≈29h
Fine	400k	0.35	≈51h
Very Fine	550k	0.3	≈69h

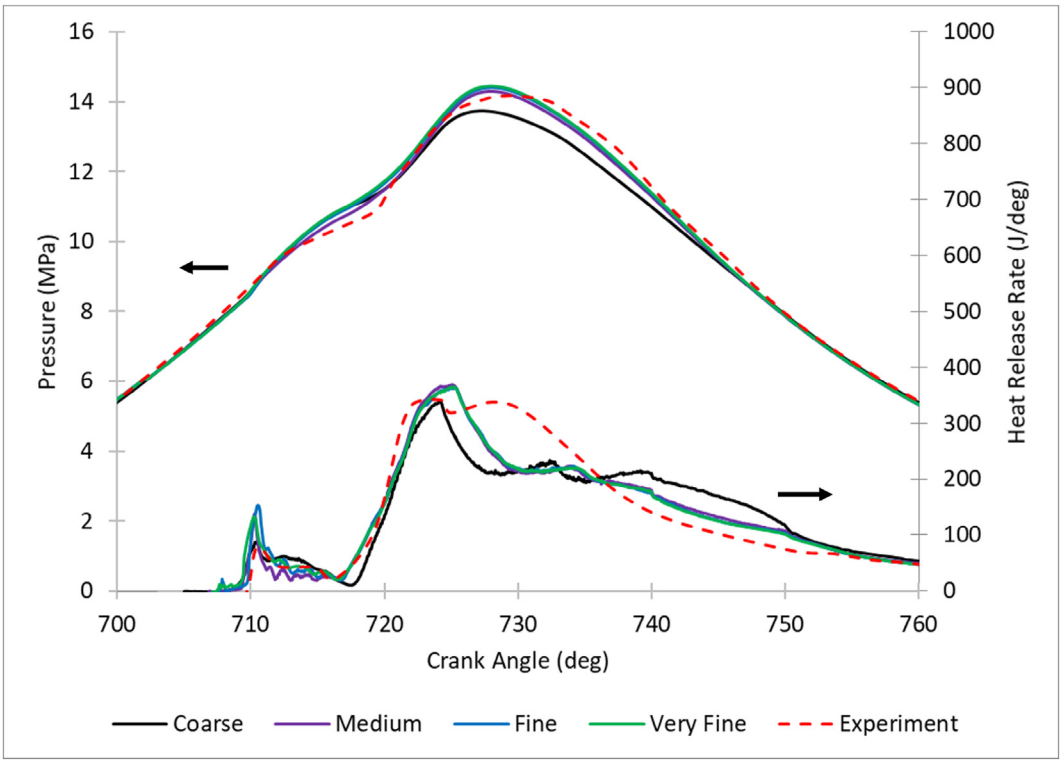

Fig. 3 – Pressure and heat release rate predictions and mesh sensitivity study for the 18% EGR test case with comparison to experimental data.

during the diesel injection where the medium grid has a similar peak HRR but lower level of mixing controlled diesel combustion than the fine grid which leads to lower pressures. The difference between the fine and very fine grids is even smaller with the only significant change being a slightly earlier diesel ignition which leads to a lower peak diesel HRR in the very fine grid. This could be due to grid effects but may simply be due to the cycle to cycle variation which the discrete

Please cite this article as: Ramsay CJ, Dinesh KKJR, Numerical modelling of a heavy-duty diesel-hydrogen dual-fuel engine with late high pressure hydrogen direct injection and diesel pilot, International Journal of Hydrogen Energy, https://doi.org/10.1016/j.ijhydene.2023.09.019

phase model can cause. Results indicate that the RANS scales are adequately resolved when using a maximum cell size of 0.35 mm, in line with the expected 0.1–1 mm minimum length scale discussed in the literature [64–67], so for the remainder of this study the 0.35 mm fine mesh is used and deemed insensitive to further mesh refinement.

Assessing the CFD modelling framework's ability to predict pollutant emissions under differing conditions is important for gaining insight into various engine operating strategies. As pollutant soot and NO_x predictions are decoupled from the main flow solution the absolute values predicted are not of much importance, but the trends predicted should still follow those of the experimental data. As can be seen in Fig. 4, the overall trends of both NO_x and soot emission as EGR rate is increased are predicted fairly well with NO_x showing a decrease between 0% and 25% EGR rates and soot showing an increase. The percentage decrease in NO_x is also well predicted with simulations showing a decrease of 82% between 0% and 25% EGR rates and experiments showing a decrease of 80%. The findings are in line with the expected effect of EGR on NO_x development, whereby reduction in oxidiser leads to lower combustion temperatures which is further aided by the dissociation of H_2O and CO_2 during combustion and the higher heat capacity of the exhaust gases acting as heat sinks. The percentage increase in soot is underpredicted in comparison to experiments which likely indicates a need to tune model parameters, include a soot mechanism in the chemical kinetics, improve initial charge composition as EGR rate is increased or various other factors. However, the general increasing trend of soot emissions being captured is deemed

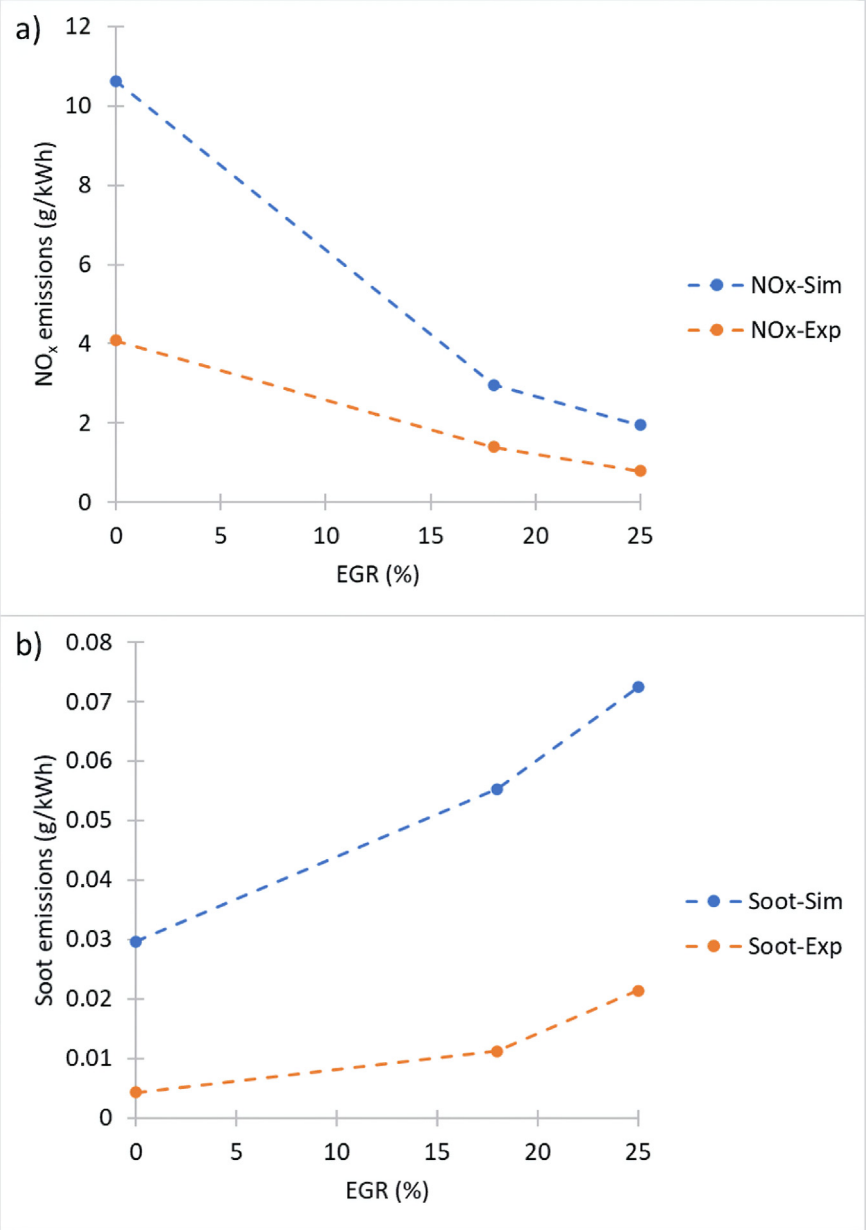

Fig. 4 – Pollutant trend predictions of a) NO_x and b) soot at EVO for increasing levels of EGR compared with experimental measurement.

Please cite this article as: Ramsay CJ, Dinesh KKJR, Numerical modelling of a heavy-duty diesel-hydrogen dual-fuel engine with late high pressure hydrogen direct injection and diesel pilot, International Journal of Hydrogen Energy, https://doi.org/10.1016/j.ijhydene.2023.09.019

sufficient for the current work. Increased soot emissions with increased EGR use is expected due to the decrease of oxygen availability leading to an increase in fuel rich areas and thus soot formation as well as the reduced in-cylinder temperatures being better suited for soot development.

Ideally validation would have been carried out using a dual direct injection diesel-hydrogen engine, however, the literature is distinctly lacking in this regard as the only suitable experimental hydrogen study found [30] uses a non-matching diesel-hydrogen injector hole arrangement which largely targets premixed hydrogen combustion and would increase computational costs greatly as the domain couldn't be periodically reduced. The diesel-natural gas engine model validation should be adequate as the chemical mechanism contains a detailed hydrogen oxidation mechanism [63] and both the medium and fine mesh showed good agreement with experimental results indicating that the fine mesh should be able to adequately resolve the higher velocity and temperature gradients present during hydrogen injection and combustion. Using this setup also means that an in-depth comparison of methane and hydrogen HPDI can be made and key differences identified. For further details about the full modelling setup and validation please see the previous work carried out by the author [51].

Some minor modification are made to the model in the upcoming analysis compared to the previous validation. Injection pressure is increased to 40 MPa to ensure the nozzle is choked during all operating points. Conversely, nozzle diameter is reduced to 0.577 mm to keep mass flow rates equivalent to the validation case (for methane; hydrogen will always be less due to density differences) as this should keep combustion phasing somewhat similar. This ensures a fairer comparison between cases as steady mass flow rate will not change during a given case due to unchoking of the nozzle and also represents an injection pressure and nozzle diameter which should be targeted in practical applications. All HL cases use a total energy of 1304 J (diesel + gaseous fuel) and all LL cases 434 J. While the HL case uses the same initial absolute pressure (3.82 bar) and temperature (431 K) as the validation simulations unless stated otherwise, the LL case uses slightly lower initial absolute pressure (3 bar) and temperature (390 K) to model what would be expected in a practical engine setup where turbocharging level is used as a way to control load in conjunction with smaller fuel injections. At this point it's likely good to point out that the IVC provided by the experimental validation study is further into the compression stroke than is standard (90°CA after bottom dead centre). So while it may seem as if the initial turbocharging levels are quite high they equate to effective compression ratios of 38.7 at HL and 30.4 at LL which are fairly standard for diesel engine operation. From here on it's simply assumed that the engine operates on a late intake valve close cycle similar to some Miller cycle implementations.

3. Results and discussion

Combustion, performance and emissions characteristics of the two gaseous fuels are examined across 3 gaseous energy shares (95%, 97% and 99%) and at high and low load conditions in a dual-fuel compression ignition engine with late HPDI of the gaseous fuels and diesel pilot. It's worth mentioning that real-world diesel injectors may struggle to properly inject the small volumes of fuel required at the likes of LL 99% energy share [68], but this problem is outside of the scope of the current study.

The first two tests simulate equivalent injection conditions (same injection pressure and diameter) for hydrogen and methane which leads to a slightly lower energy flow rate and longer duration for the hydrogen injection (case 0 and case 1), while the second set changes various injection parameters such that energy flow rate and duration of the hydrogen injections are equivalent to the baseline methane case (case 2, 3 and 4). Table 6 outlines the injection conditions for the test cases, where P_0 is the upstream injection pressure, D_e is the exit nozzle diameter and $\dot{m}$ is the choked mass flow rate.

3.1. Combustion trends at high and low load

We first compare the combustion of methane and hydrogen at 95% gaseous energy share as consistent and stable combustion is present at both load conditions. From observation of the 95% energy share heat release rate graphs, top row of Fig. 5, it is clear that the diesel pilot adequately ignites the gaseous injections for both fuels almost instantly upon their injection into the combustion chamber. Due to hydrogen's lower minimum ignition energy this ignition occurs about 0.3°CA earlier for the hydrogen injections compared to methane. Peak HRR and in-cylinder pressure is higher for the hydrogen cases, but the fall-off from peak HRR occurs earlier and HRR levels remain much lower for the remaining power stroke compared to methane due to hydrogen's much shorter oxidation pathway.

Next we address the change in combustion characteristics as gaseous energy share is increased. From observing the HRR and pressure curves presented in Fig. 5 it can be seen that increasing gaseous energy share makes very little difference to combustion characteristics at HL for either fuel or at the varying injection conditions. This is because the reduced volume diesel pilot continues to produce enough heat to ignite the gaseous injection. This is evidenced by the very similar ignition delays of the gaseous jet observed across all HL cases. A completely different story is told at LL due to the smaller pilot injection compared to HL. At 95% gaseous energy share the diesel pilot adequately ignites the jet with very similar jet ignition delays to the HL cases. However, further decrease of the pilot volume leads to much longer gaseous jet ignition delays at 97% energy share leading to high levels of premixed combustion and high pressure rise rates/HRR peaks. Hydrogen won't produce soot/CO/UHCs like diesel during this type of combustion mode, however, hydrogen's wide flammability limits and very high burning velocity mean that too much fuel is likely to combust over a very short period of time. This type of combustion is undesirable as the rapid and rich premixed combustion which occurs generally leads to high engine noise and possibly damage, while also causing difficulties with controlling engine operation as the ignition timing becomes unpredictable. NO_x emission during this type of combustion mode may be lower than the high temperature combustion which occurs in a non-premixed flame, however, this will only

Please cite this article as: Ramsay CJ, Dinesh KKJR, Numerical modelling of a heavy-duty diesel-hydrogen dual-fuel engine with late high pressure hydrogen direct injection and diesel pilot, International Journal of Hydrogen Energy, https://doi.org/10.1016/j.ijhydene.2023.09.019

Table 6 – Injection conditions for methane-hydrogen comparisons.

Case	Fuel	P_0 (MPa)	D_e (mm)	$\dot{m}$ (kg/s)	Energy flow rate (MJ/s)	Energy per gaseous injection (J)		
						95%	97%	99%
						HL | LL	HL | LL	HL | LL
0	CH_4	40	0.577	0.013900	0.695	1236 | 412	1265 | 422	1291 | 430
1	H_2	40	0.577	0.005042	0.605	1236 | 412	1265 | 422	1291 | 430
2	H_2	46	0.577	0.005792	0.695	1236 | 412	1265 | 422	1291 | 430
3	H_2	40	0.619	0.005792	0.695	1236 | 412	1265 | 422	1291 | 430
4	H_2	80	0.437	0.005792	0.695	1236 | 412	1265 | 422	1291 | 430

be the case if the amount of premixing is somewhat controlled to not allow for the majority of the fuel volume to burn in a much shorter period. The inconsistent and difficult to control engine operation is highlighted by the wide variance in ignition delays observed between cases at LL 97% energy share with the likes of C3, which is still a similar setup to the other cases, essentially showing no combustion of the hydrogen jet. Similar to this case, all 99% LL cases show almost no hydrogen combustion due to the much reduced diesel injection providing too little energy for ignition of the injected gaseous jet.

Clearly considerable improvements need to be made at very high gaseous substitution levels when load is reduced but the results at HL are promising and show the potential of this type of engine operation.

3.2. *Combustion process in a late gaseous HPDI compression ignition engine with diesel pilot*

Fig. 6 provides a breakdown of the general combustion process in the engine when the diesel pilot adequately ignites the hydrogen injection and the following discussion provides a detailed explanation of the processes occurring.

The time series temperature contours shown in Fig. 7 highlight the differences in the combustion process at HL 95% energy share between the two fuels (C0 and C1 compared). Clearly the diesel injection provides an adequately high temperature region in the vicinity of the injected gases trajectory close to the injectors (715°CA contours). Upon contact with this region the gas jet quickly ignites with little to no premixed combustion present, the rich lower temperature core stays intact throughout, 716°CA - 717°CA contours, with no early HRR spike and a non-premixed diffusion flame forms. The lack of premixed combustion is mostly due to the lack of air entrainment because of the underexpanded flow structures close to the injector and rapid ignition once entrainment begins.

The formation of a flame indicates the end of the ignition delay phase and beginning of the free-jet combustion phase (716–721°CA contours). The higher injection velocity of the hydrogen (higher speed of sound) leads to a much faster penetration rate than the methane which likely contributes to the faster ignition and is certainly a factor in the higher pressure rise rate, and climb to peak HRR, due to the rate of mixing with oxidiser being much higher as the flame penetrates the chamber. The non-premixed flame is also thicker in the hydrogen case as evidenced by the reduced low temperature core width and wider high temperature region surrounding it on either side and in-front (721°CA contours). This is partly due to hydrogen's higher mass diffusivity and thus further reach with regard to mixing but is mostly due to its much wider flammability limit allowing for far richer combustion towards the core and leaner combustion towards the outer edge of the jet. This is also the reason for the higher peak HRR value in the hydrogen cases which occurs just before the jets contact with the chamber wall. The peak HRR correlates with the point at which the non-premixed flame is largest, i.e. before the leading edge is quenched by the chamber wall (721°CA vs. 724°CA contours), and as noted hydrogen's flame is much wider than its methane counterparts. This peak in HRR also occurs earlier for the hydrogen cases due to the increased penetration rate and thus earlier contact with the chamber wall.

Upon contacting the wall the front of the flame quenches and HRR begins to fall due to a smaller flame volume and an accumulation of fuel which is too rich to combust at the rate it was previously, indicating the end of the free-jet combustion phase and beginning of the wall-jet combustion phase (724°CA-735°CA contours). This process is very pronounced for the methane case where a clear low temperature region forms around the piston bowl walls. However, due to hydrogen's far lower quenching distance and wider flammability limit combustion is still occurring along the wall, although at a reduced rate compared to the free-jet combustion. The impinging jets momentum forces fuel along the walls in all directions; into the piston bowl and back towards the injectors, laterally towards other sectors of the chamber and towards the top cylinder and liner walls. This spreading of the fuel allows for adequate mixing of fuel and oxidiser which leads to a levelling off in HRR at a moderate level, and is best shown in the HL HRR graphs as the injection ends too early to see this at LL. As combustion is focussed within the piston bowl a high temperature area develops which is especially apparent for hydrogen due to its ability to burn at much higher fuel-air equivalence ratios, and can be clearly seen in the 735°CA contours. This increase in fuel utilisation leads to higher HRR levels during the wall-jet combustion for the hydrogen cases compared to methane. During this phase, and later after the end of injection, spreading out of the fuel and flame front is apparent and interaction with fuel from other injectors is likely and may enhance the combustion rate in some cases. This can be seen somewhat in the climbing HRR towards the end of the phase. This process is more likely for hydrogen which spreads faster because of the increased jet velocity and thus increases the chance of meeting fuel from

Please cite this article as: Ramsay CJ, Dinesh KKJR, Numerical modelling of a heavy-duty diesel-hydrogen dual-fuel engine with late high pressure hydrogen direct injection and diesel pilot, International Journal of Hydrogen Energy, https://doi.org/10.1016/j.ijhydene.2023.09.019

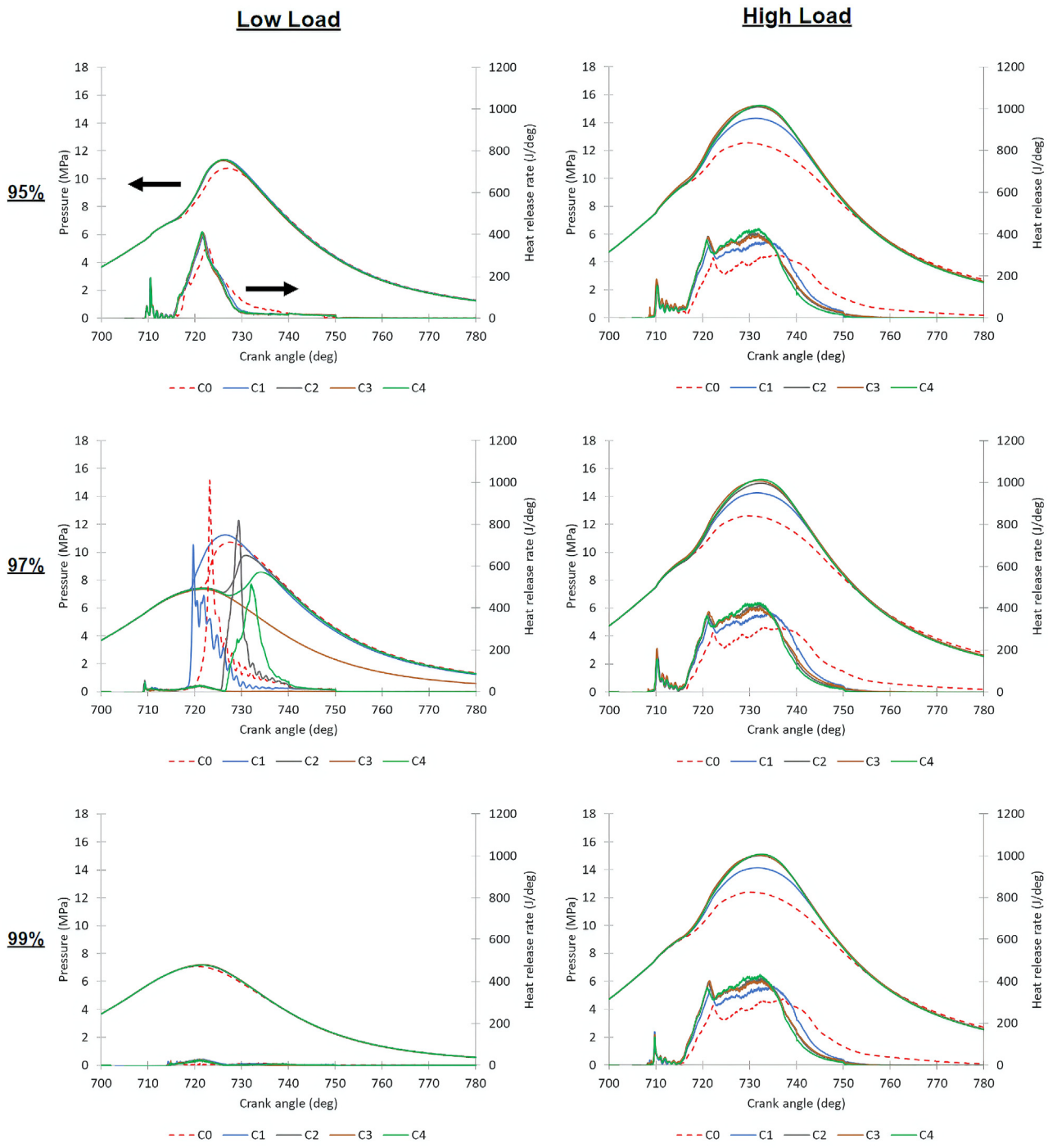

Fig. 5 – Calculated pressure and HRR trends for methane-hydrogen comparisons at 95%, 97% and 99% gaseous energy shares.

other sectors injectors before the end of the injection event while the jets still have a high momentum.

As the injection ends HRR falls off rapidly signalling the end of the wall-jet combustion phase and start of the late combustion phase (740°CA-760°CA contours continuing until EVO). Even though the hydrogen injection ends later, the fall off in HRR occurs earlier and is much more rapid than the methane case. This is due to the oxidation of the remaining UHCs producing heat when methane is used, whereas comparatively almost all of the hydrogen has been oxidised due its much shorter and simpler chemical breakdown pathway. In general, the rich core stays intact for a short while after the end of injection for both fuels but over time it begins to decay until eventually being engulfed by the remaining flame (740°CA contours). There is often a secondary peak right before the fall off in HRR which is due to the rapid combustion that occurs when the jet core collapses which is enhanced by the wall-jet/combined injector jets convection into this

Please cite this article as: Ramsay CJ, Dinesh KKJR, Numerical modelling of a heavy-duty diesel-hydrogen dual-fuel engine with late high pressure hydrogen direct injection and diesel pilot, International Journal of Hydrogen Energy, https://doi.org/10.1016/j.ijhydene.2023.09.019

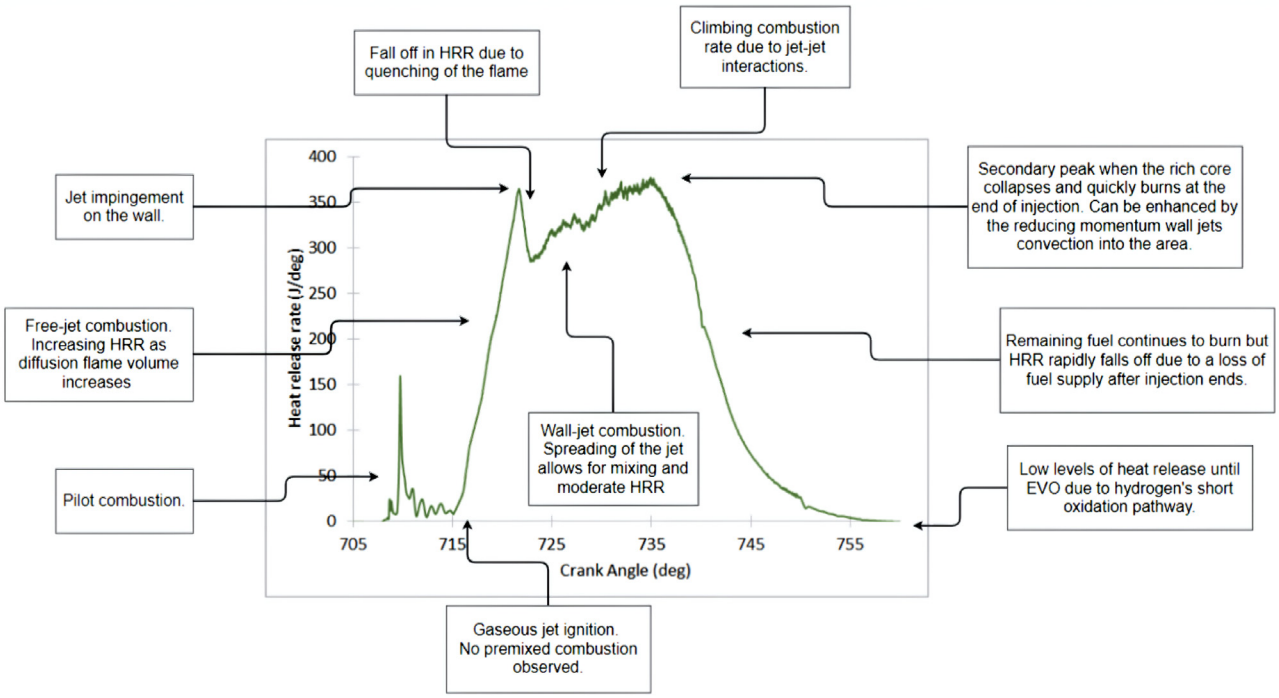

Fig. 6 – Description of the general combustion process in a dual direct injection hydrogen-diesel dual-fuel compression ignition engine (high load 95% HES case 1 shown).

region. Small amounts of combustion continue for the remainder of the power stroke, as evidenced by the fairly high temperature regions. It's clear however that both from the quickly reducing temperatures in the hydrogen cases (760°CA contours), and much lower HRR that greater amounts of combustion are occurring in the methane cases at this stage due to the aforementioned oxidation of UHCs. There is however still a low temperature region formed in the piston bowl region for the methane case, where there is a rich pooling of UHCs where combustion cannot reach, which is not present for the hydrogen case (760°CA contours). Minimal interaction of the hydrogen close to the cylinder liner and the hydrogen in the piston bowl/injection region is observed after the injection event ends, with two clear separate zones of recirculation forming.

Fig. 8 depicts the impact of the impinging hydrogen jet on the flow field during and after the gaseous injection event. Initially, prior to impingement, the free-jet displaces the air around it, pushing air both ahead of itself towards the piston bowl/chamber liner and also around itself and back towards the injectors. This is partly attributed to the minimal air entertainment in the early development of the jet, as evidenced by the lack of premixed combustion and rich core. Upon impingement, the jet curls up in the piston bowl, spreading out as it impinges on the wall. The momentum of the jet pushes hydrogen along the wall in all directions. Recirculation zones form in the piston bowl and towards the top of the chamber near the liner which slows the rate of combustion as fuel rich areas form. After a time the outward spreading leads to contact of the jet with those from other injectors, and this interaction slows the lateral movement but further propels the jet back up the slope towards the injectors. Finally the injection event ends and the lack of momentum and decaying core leads to high levels of recirculation along the trajectory of the jet which combines with the fuel which was pushed back towards the injectors. This process enhances the combustion rate somewhat and also leads to the formation of a large high temperature zone as can be seen in the 740°CA/750°CA contours in Fig. 7.

The temperature contours shown in Fig. 9 show the stark contrast between the ignition and combustion process as gaseous energy share is increased at LL (C0 and C1 compared). At 99% the diesel injection offers so little temperature rise that by the time the gaseous injection begins there is essentially no hot products combusting (top right 720°CA) leading to no ignition for either fuel. At 97% operation improves a lot compared to 99% as the pilot provides enough energy to ignite the jet. However, the ignition is delayed as shown by the 720°CA methane contour (same is observed for hydrogen at earlier crank angles than shown) which also reduces initial jet

Please cite this article as: Ramsay CJ, Dinesh KKJR, Numerical modelling of a heavy-duty diesel-hydrogen dual-fuel engine with late high pressure hydrogen direct injection and diesel pilot, International Journal of Hydrogen Energy, https://doi.org/10.1016/j.ijhydene.2023.09.019

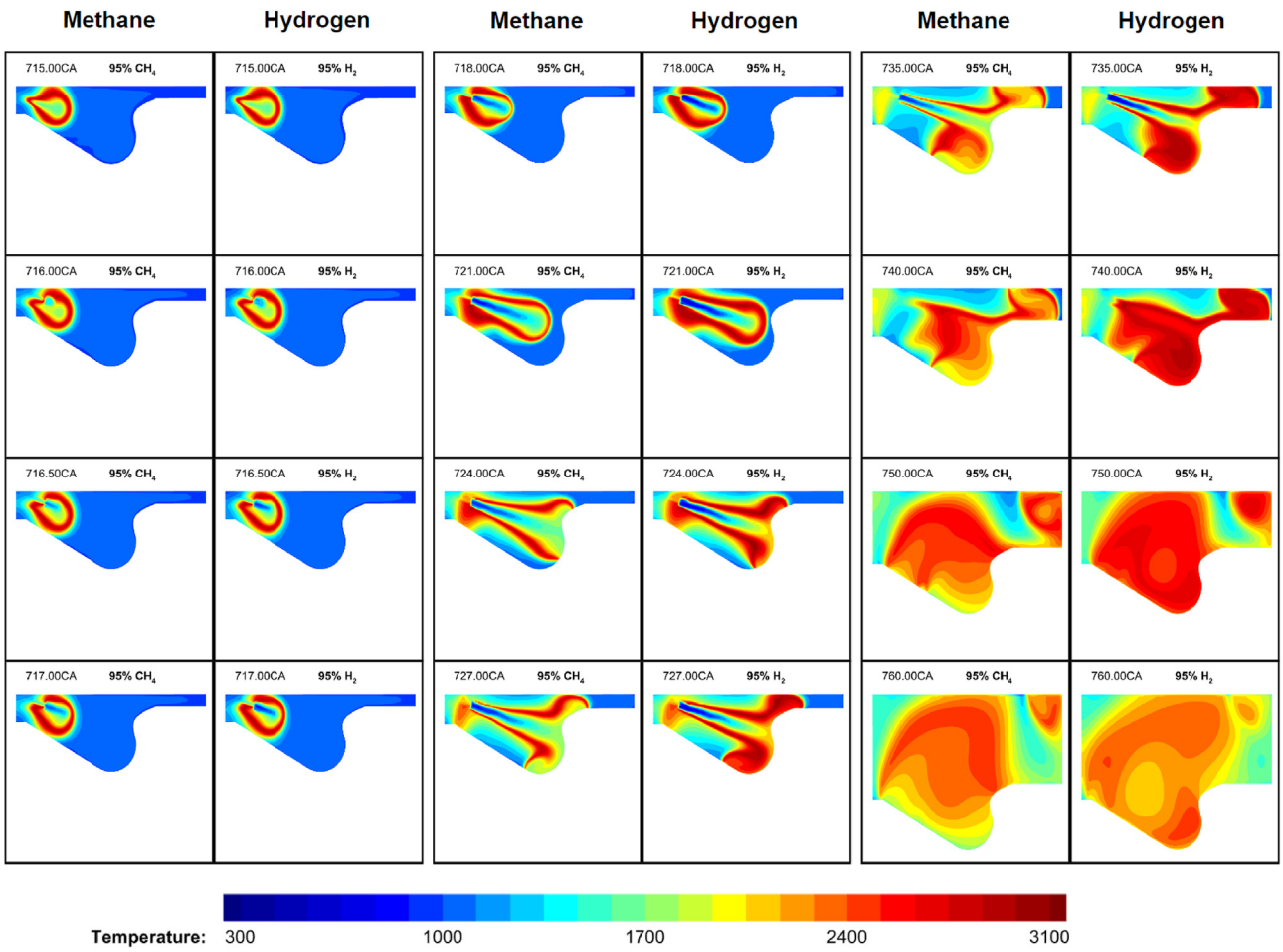

Fig. 7 – Temperature contours for methane and hydrogen at high load 95% gaseous energy share (case 0 & 1).

penetration as the acceleration of the jet via combustion occurs later than in the 95% cases. This late ignition leads to a much higher gaseous fuel burning rate early in the injection and can be observed in the 730°CA and 740°CA contours where the temperatures in the centre of the sector are higher than the same regions at 95% energy share. The reduced penetration rate also contributes to the more focussed central combustion site as there is greater fuel dispersion which is why the flame is somewhat wider at 97% energy share. There are also lower temperatures in the near injector region throughout at 97% energy share both because the initial combustion occurs slightly later into the gaseous jets trajectory and also due to the reduction in pilot volume. These contours highlight the importance of the pilot injection and the need to optimise its volume and ignition timing to ensure that an adequately high temperature region is present when the gaseous injection begins.

3.3. *Performance and emission characteristics*

At this point we note that thermal efficiency is calculated using the gross indicated work, i.e. integrating only pressure/volume between IVC and EVO, thus the values are somewhat higher than would be expected in a practical engine as the various losses are not accounted for. The engine operating on an overexpanded cycle (50° longer expansion stroke compared to compression) also contributes. However, trends captured are more important than the absolute value so this should not be of concern. The same can be said for presenting the likes of work or power output as the gross indicated version of these

Please cite this article as: Ramsay CJ, Dinesh KKJR, Numerical modelling of a heavy-duty diesel-hydrogen dual-fuel engine with late high pressure hydrogen direct injection and diesel pilot, International Journal of Hydrogen Energy, https://doi.org/10.1016/j.ijhydene.2023.09.019

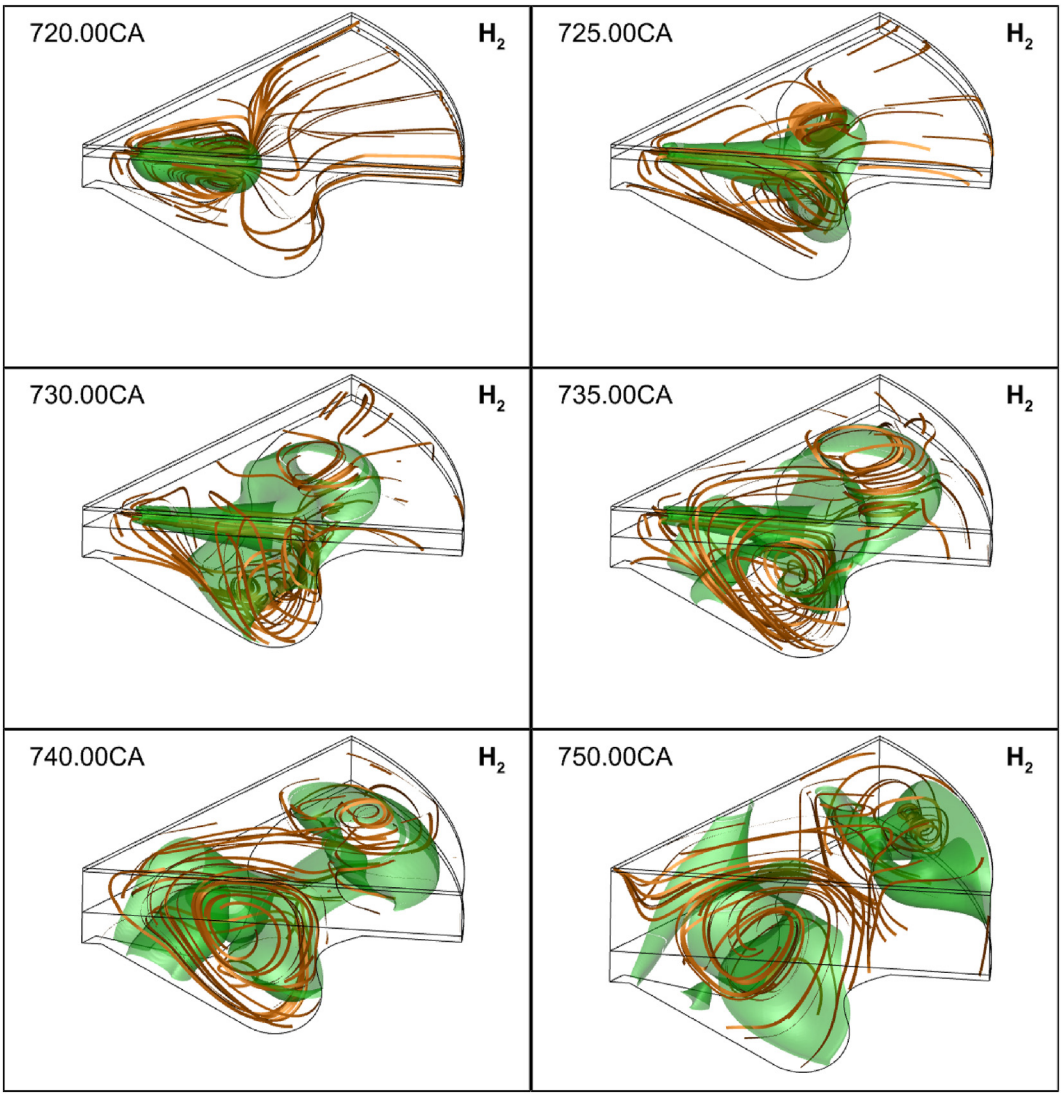

Fig. 8 – Streamlines and hydrogen isosurface at a mass fraction of 0.001 showing the jet induced flow field at HL 95% HES.

quantities are linearly linked to the gross indicated thermal efficiency.

Fig. 10 presents the calculated emissions and thermal efficiency of each case at HL. Clearly as expected hydrogen leads to much higher NO_x emissions than methane due to the much faster and higher temperature combustion observed, however, the reduction of supplied carbon leads to a considerable decreases in all carbon based emissions. Due to the high fuel burning efficiency at HL this also means hydrogen emissions are lower in the hydrogen cases as the breakdown of UHCs ends up outweighing any unburned injected hydrogen fuel (this could also be an indication that the fuel mechanism needs to be improved, but nonetheless indicates high fuel utilisation in the hydrogen cases). Performance also sees a small uplift across most hydrogen cases compared to methane. The performance increase is smaller than might be expected when comparing the pressure graphs but this is due to the increased late power stroke pressures in the methane cases as the oxidation of UHCs continues to produce heat, and therefore work, all the way up to EVO.

There is relatively little change between each hydrogen case across all the energy shares. The two key points to note are the injection rate increase leading to increased NO_x emissions due to the increased rate of burning causing higher in-cylinder pressures and temperatures, and very similar performance (in some cases reduced) compared to the original hydrogen case. This poor performance trend can likely be somewhat attributed to the reduction in free jet combustion

Please cite this article as: Ramsay CJ, Dinesh KKJR, Numerical modelling of a heavy-duty diesel-hydrogen dual-fuel engine with late high pressure hydrogen direct injection and diesel pilot, International Journal of Hydrogen Energy, https://doi.org/10.1016/j.ijhydene.2023.09.019

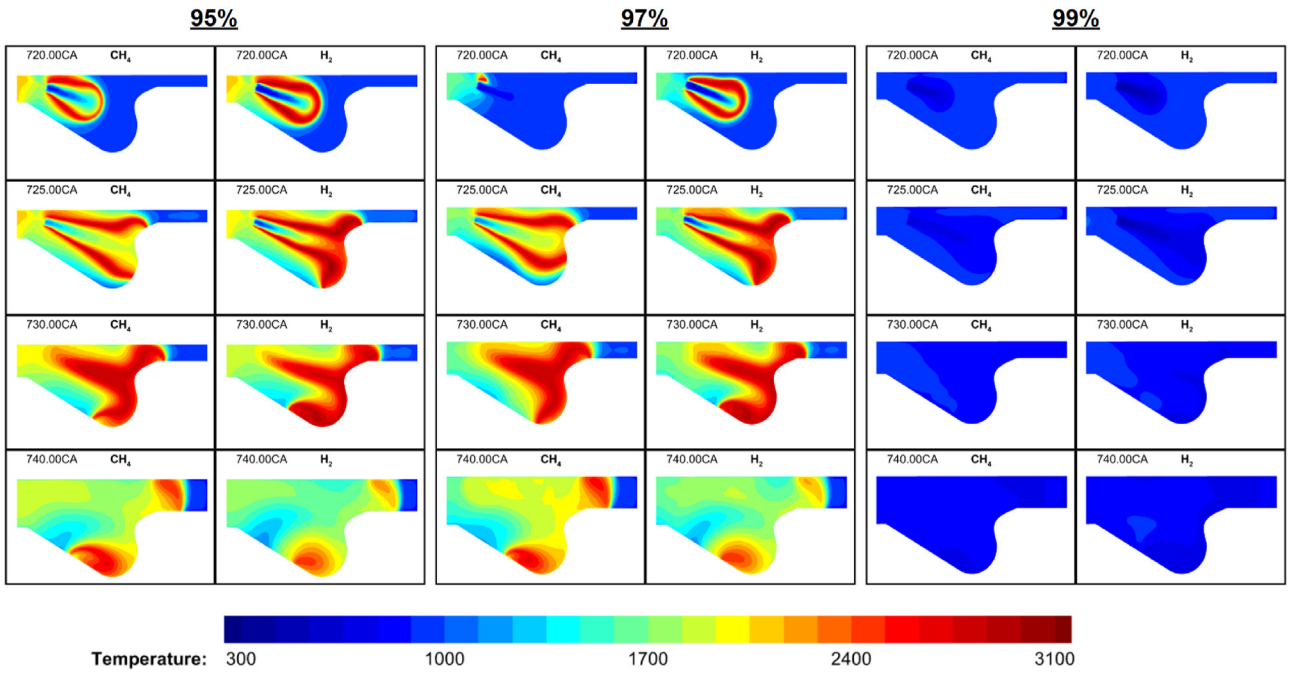

Fig. 9 – Temperature contours comparing methane and hydrogen at low load 95%, 97% and 99% gaseous energy share (case 0 & 1).

occurring as the jet contacts the chamber wall earlier. This indicates C2, C3 and C4 are not effective strategies going forwards.

However, one of the significant findings is the decrease in UHC emissions as the injection rate is increased at 95% HES. Not only do the higher temperatures aid in this process but the increased convection due to the higher jet momentum and larger mach disk diameters in C2, C3 and C4 improve the mixing in the near injector area leading to improvements to the pilot burning. Pilot combustion products also often get entrained in the jet (also improved by momentum/diameter) and are burned as it penetrates the chamber further improving utilisation. This process is shown in Fig. 11 where it is clear that in C1 more of the UHCs are accumulating in the near injector region whereas in C3 more UHCs are entrained in the hydrogen jet and are being pushed into the piston bowl. The entrained UHCs then burn efficiently with the hydrogen jet as they penetrate the chamber. At higher energy shares, where the pilot penetration is reduced, poorer pilot burning is sometimes observed leading to higher UHC emissions due to the combustion products getting stuck behind the injector. This is a result of the increased mach disk/core length reducing gaseous jet combustion close to the injector compared to lower pressure ratio/nozzle diameter cases and in some cases the higher momentum jet pushes more air around itself and back towards the injector area, essentially trapping the already poorly penetrating pilot products behind the jet in the injector region (see Fig. 8).

Comparing the contours for C1, C2, C3 and C4 at HL 99% HES, Fig. 12, it is clear that simply increasing injection rate does not necessarily improve combustion and mixing of the hydrogen with oxidiser. In fact, the jets increased momentum causes the hydrogen, which in C1 gets caught close to the liner, to deflect off the walls and move back towards the injector region where there is a lack of oxidiser because of the combustion which already took place there. The highest NO_x levels occur close to the top of the chamber along the trajectory of the hydrogen injection and to a lesser extent along the piston bowl walls. This is amplified as the injection rate is increased as the combustion is less spread out compared to C1 with the liner deflected hydrogen likely also enhancing the NO_x production in the region. These contours clearly indicate that slowing the hydrogen injection rate or increasing the coverage/mixing of the injection should be an effective way to

Please cite this article as: Ramsay CJ, Dinesh KKJR, Numerical modelling of a heavy-duty diesel-hydrogen dual-fuel engine with late high pressure hydrogen direct injection and diesel pilot, International Journal of Hydrogen Energy, https://doi.org/10.1016/j.ijhydene.2023.09.019

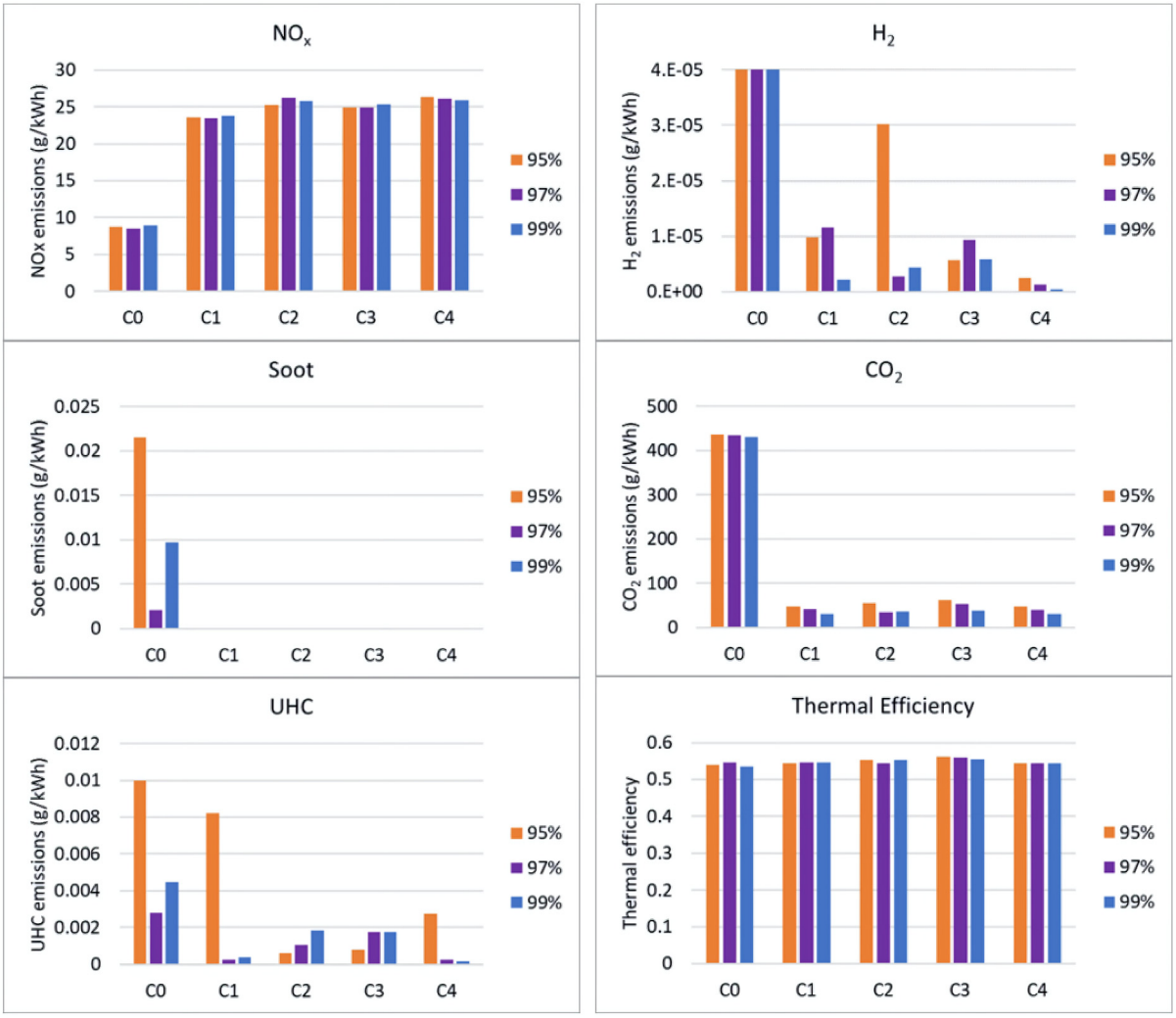

Fig. 10 – Calculated HL thermal efficiency and NO_x, soot, UHC, CO_2 and H_2 emissions at EVO for 95%, 97% and 99% gaseous energy shares - methane hydrogen comparisons.

control NO_x while also potentially improving hydrogen utilisation. The increased CO_2 levels shown at the top left of the contours are a clear indication of improved pilot utilisation when jet momentum is increased leading to improved mixing of the pilot combustion products with higher cylinder temperatures also contributing. This improved mixing and utilisation of UHCs is reflected in the soot contours also, where for the most part soot levels reduce with the increase in jet momentum due both to less initial formation and greater oxidation.

Fig. 13 presents the calculated emissions and thermal efficiency of each case at LL. Comparing the 95% methane and hydrogen cases it is clear that NO_x increases while carbon based emissions generally decrease similar to the higher load condition. UHCs do not tend to follow the same trend which is due to a similar process to the one shown in Fig. 11. The reduced LL pilot penetration means pilot combustion products get caught behind the injector and the reduced penetration of the gaseous injection means the flame struggles to curl up in the piston bowl and make it back towards the injector and burn the pilot fuel in the same way it does at HL (compare 740°CA contours in Fig. 7 with Fig. 9). This means UHC oxidation is much more reliant on late power stroke combustion which is much poorer for hydrogen cases. Performance tends to decrease compared to methane due to the overall poorer fuel utilisation.

At 97% energy share the unstable combustion leads to far poorer fuel utilisation which causes high hydrogen and UHC emissions combined with a reduction in performance when compared to 95% energy share. NO_x emissions do tend to

Please cite this article as: Ramsay CJ, Dinesh KKJR, Numerical modelling of a heavy-duty diesel-hydrogen dual-fuel engine with late high pressure hydrogen direct injection and diesel pilot, International Journal of Hydrogen Energy, https://doi.org/10.1016/j.ijhydene.2023.09.019

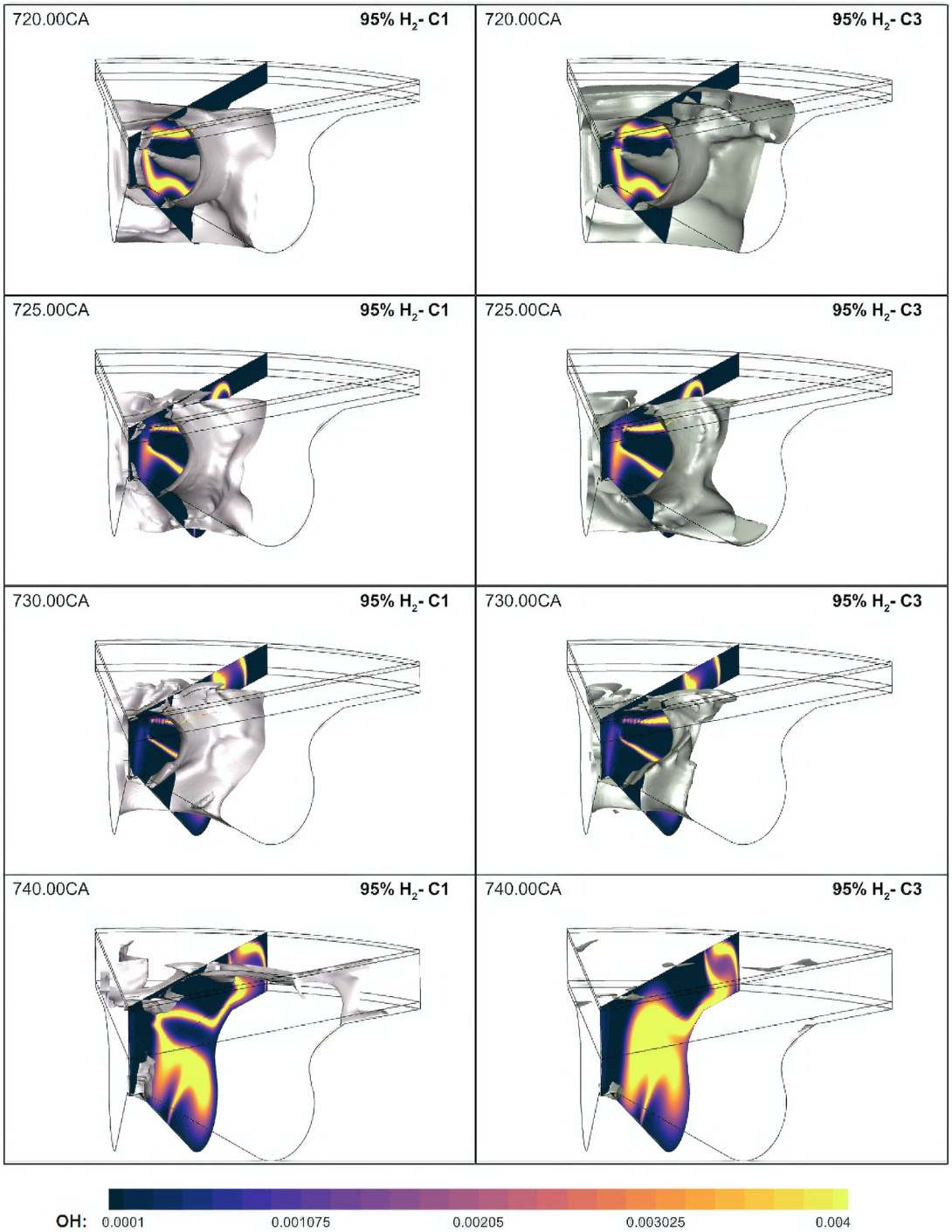

Fig. 11 – UHC isosurfaces at 0.05% mass fraction with OH mass fraction contours at 95% HES HL cases 1 and 3.

reduce, but this is mostly due to the delayed onset of combustion and lower levels of fuel burning reducing temperatures. This is not the correct way to go about reducing NO_x but does indicate that a later injection timing should be beneficial given adequate ignition can be achieved and also implies that premixed combustion modes may offer some potential for NO_x reduction.

Clearly 99% energy share shows poor combustion all around and therefore the likes of UHC and H_2 emissions increase dramatically while thermal efficiency drops to near 0%

Please cite this article as: Ramsay CJ, Dinesh KKJR, Numerical modelling of a heavy-duty diesel-hydrogen dual-fuel engine with late high pressure hydrogen direct injection and diesel pilot, International Journal of Hydrogen Energy, https://doi.org/10.1016/j.ijhydene.2023.09.019

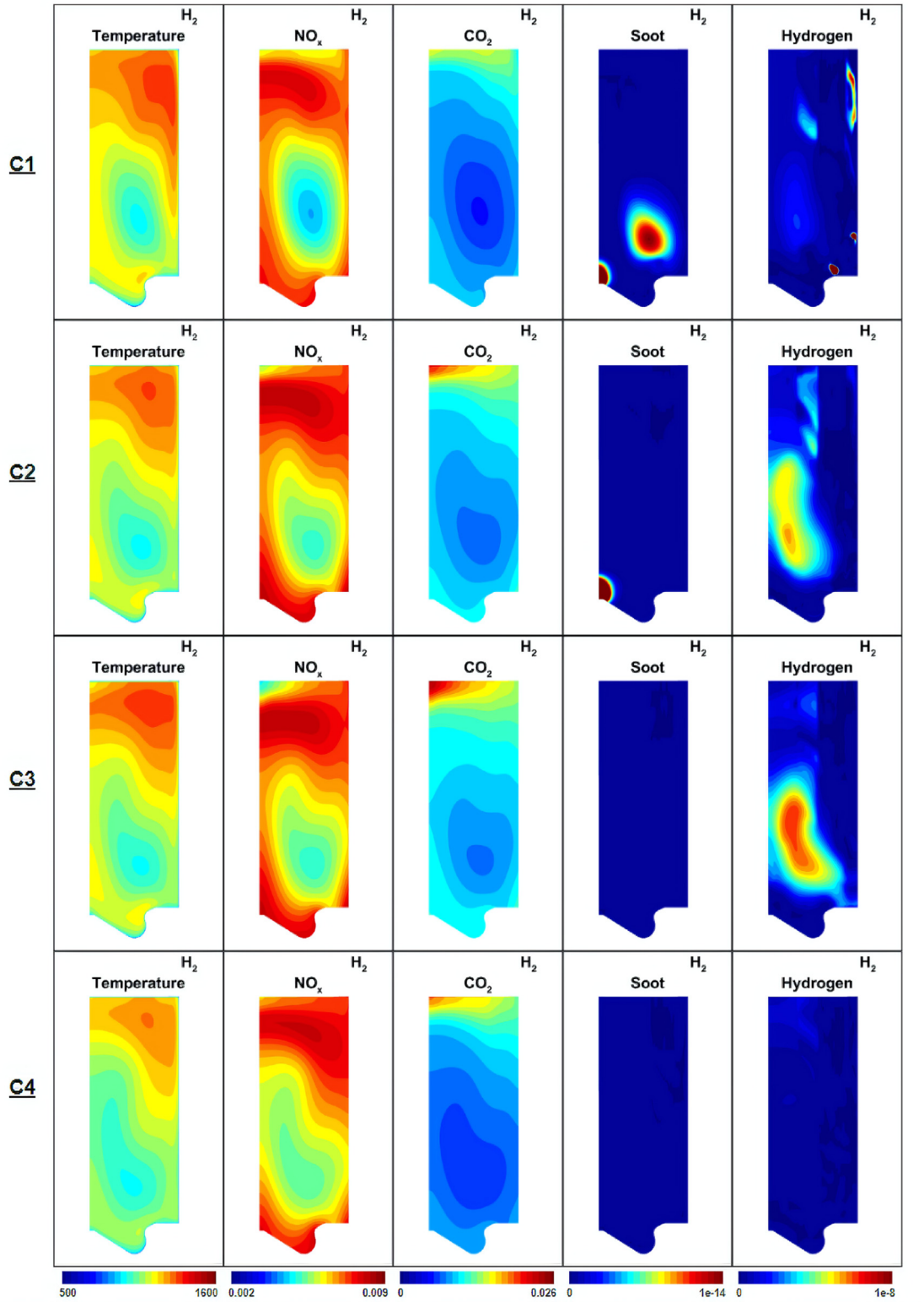

Fig. 12 – Contours of temperature, NO_x, CO_2, soot and hydrogen at EVO for HL 99% energy share of hydrogen (cases 1, 2, 3 and 4).

Please cite this article as: Ramsay CJ, Dinesh KKJR, Numerical modelling of a heavy-duty diesel-hydrogen dual-fuel engine with late high pressure hydrogen direct injection and diesel pilot, International Journal of Hydrogen Energy, https://doi.org/10.1016/j.ijhydene.2023.09.019

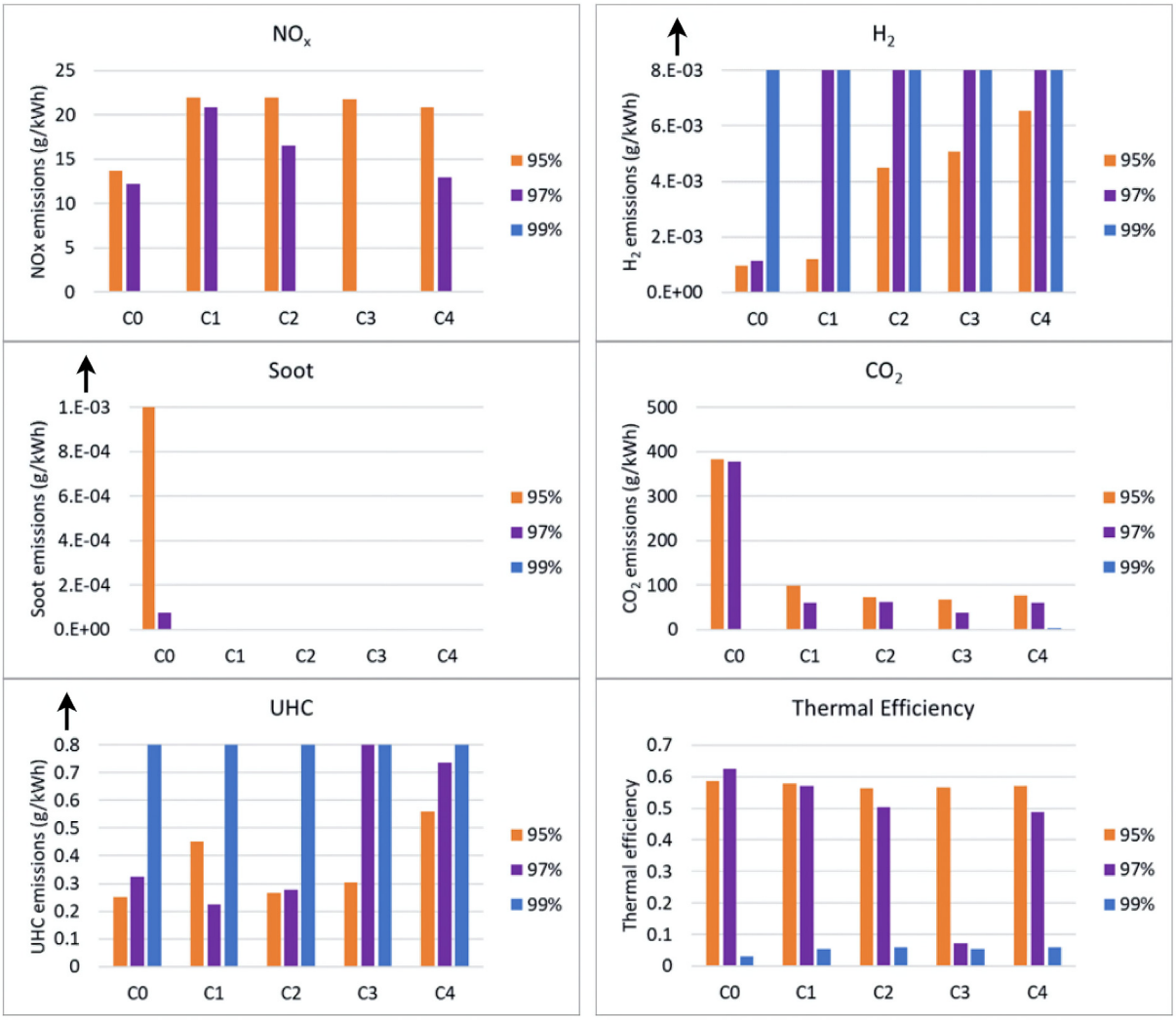

Fig. 13 – Calculated LL thermal efficiency and NO_x, soot, UHC, CO_2 and H_2 emissions at EVO for 95%, 97% and 99% gaseous energy shares - methane hydrogen comparisons.

levels. Improvements are clearly required for LL operation at this high an energy share.

Fig. 14 compares contours of temperature and emissions at EVO for the baseline methane and hydrogen cases (C0 and C1) at LL 95% and 97% energy share. Methane cases have higher late power stroke temperatures for both fuels which are higher at the lower energy share because of the early rapid premixed combustion in the 97% cases. Hydrogen cases have much higher NO_x levels which cover a larger area of the chamber due to the increased penetration and wider flame than methane. Hydrogen case CO_2 emissions are much lower than methane and they are confined to the near injector region. Both fuels show a general decrease of CO_2 at increasing energy share as a result of much poorer fuel utilisation but also due to lower carbon levels in the chamber in general. Soot is extremely low in all but the 95% methane case and it is confined to the low temperature region close to the cylinder liner and along the chamber walls close to the injector where unburned fuel has pooled. An area of unburned hydrogen forms at the top of the cylinder close to the liner in the 97% hydrogen case due to the unstable combustion meaning some of the unburned fuel gets trapped above the piston bowl at too low a temperature to burn.

Please cite this article as: Ramsay CJ, Dinesh KKJR, Numerical modelling of a heavy-duty diesel-hydrogen dual-fuel engine with late high pressure hydrogen direct injection and diesel pilot, International Journal of Hydrogen Energy, https://doi.org/10.1016/j.ijhydene.2023.09.019

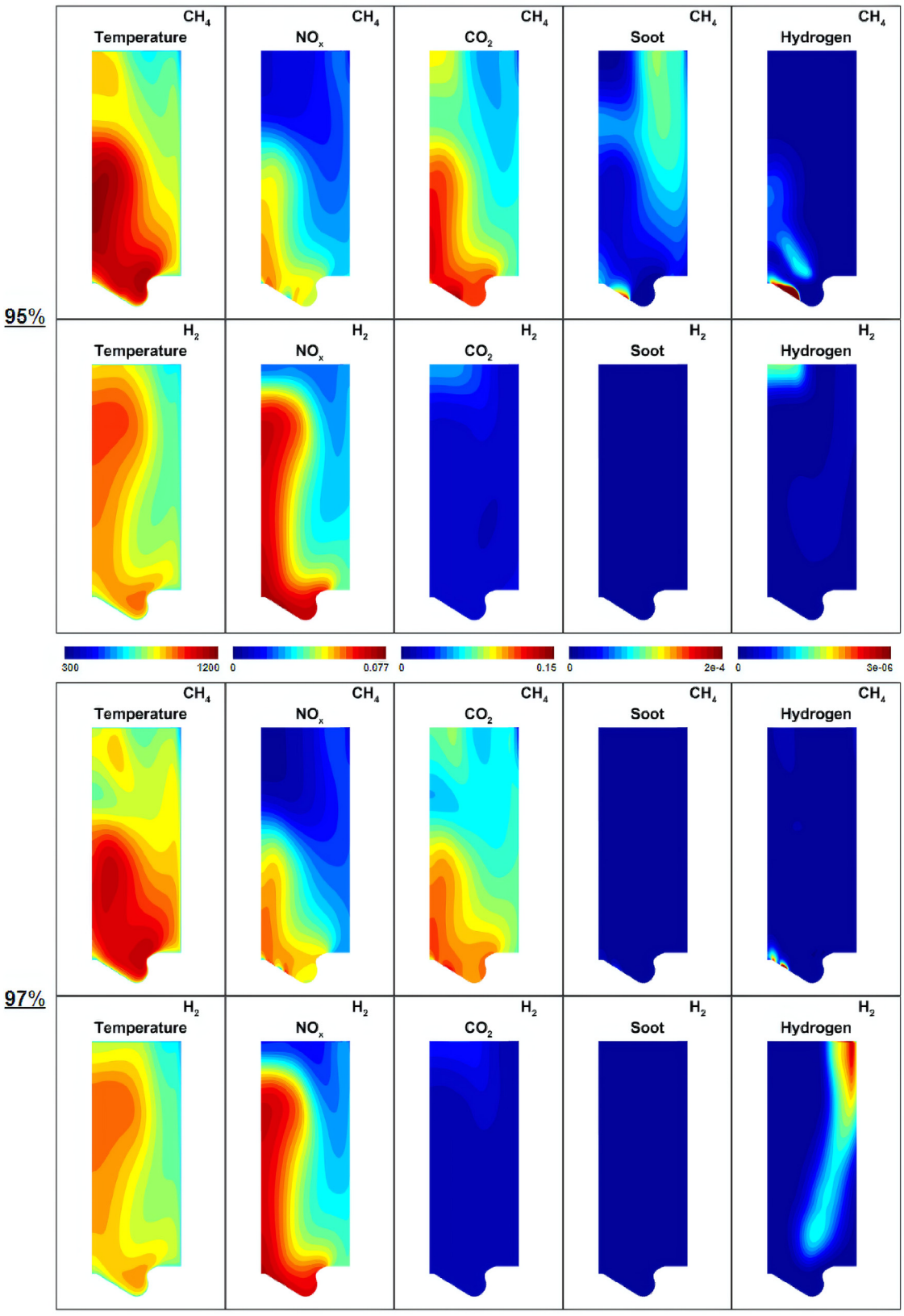

Fig. 14 – Contours of temperature, NO_x, CO_2, soot and hydrogen at EVO for LL 95% and 97% energy share of hydrogen and methane (cases 0 and 1).

Please cite this article as: Ramsay CJ, Dinesh KKJR, Numerical modelling of a heavy-duty diesel-hydrogen dual-fuel engine with late high pressure hydrogen direct injection and diesel pilot, International Journal of Hydrogen Energy, https://doi.org/10.1016/j.ijhydene.2023.09.019

4. Conclusions

A numerical study using three-dimensional computational fluid dynamics is performed to investigate a diesel pilot ignited late high pressure direct gaseous hydrogen injection engine targeting non-premixed combustion and comparisons are made with the same engine running on methane. High and low load conditions are simulated at 95%, 97% and 99% gaseous energy shares. Some of the key findings include:

- Four main phases of dual direct-injection non-premixed combustion are identified, namely: a) gaseous jet ignition delay, b) free-jet combustion, c) wall-jet combustion and d) late combustion phases.
- Ignition is generally rapid with little to no premixed combustion present with hydrogen showing shorter ignition delay times than methane.
- Free-jet combustion is the phase before the jet contacts the chamber walls with the end of the phase being signalled by the quenching of the front of the non-premixed flame at the chamber walls leading to a reduction in its volume and thus fall off from peak heat release rate (HRR). Combustion efficiency is high in this phase which is reflected in the high HRR levels observed. Generally hydrogen has a higher peak HRR due to a wider flame and faster climb to said peak as a result of faster jet penetration.
- Wall-jet combustion begins with the jets first impingement on the chamber wall. HRR initially falls off then levels out at a moderate level as fuel begins to pool along the chamber walls. The injected fuel spreads out in all directions and can come in contact with injections from other sectors of the chamber. For the most part hydrogen stays at a higher HRR than methane due to a smaller quenching distance, greater jet momentum and higher rich flammability limit.
- The late combustion phase begins after the injection event has ended and HRR begins to fall off rapidly. Hydrogen tends to have a faster fall off and lower HRR level in the late power stroke as its short efficient breakdown pathway means more fuel was utilised early in the power stroke when compared to methane which still has unburned hydrocarbons to oxidise.
- In general, hydrogen combustion leads to higher NO_x levels than methane but much reduced carbon based emissions.
- Hydrogen performance increases at high load compared to methane but decreases slightly at low load in the current setup.
- Increasing injection rate through either injection pressure or injector diameter increase leads to an increase in NO_x emissions without a performance gain and in some cases can lead to a reduction in performance. This trend can be somewhat attributed to part of the free-jet combustion phase being shifted into the wall-jet phase and thus reducing combustion efficiency.
- High load operation does not deteriorate at hydrogen energy shares (HES) up to 99% due to adequate gaseous jet ignition by the diesel pilot.
- Low load operation however does deteriorate as the diesel pilot volume reduces too much and combustion begins to become unstable when 95% HES is exceeded, causing long gaseous jet ignition delays and high levels of premixed combustion. Further increase to 99% HES leads to little to no combustion of the gaseous jet. Similar results were found for methane.

Four clear problems which need to be addressed with respect to high HES dual-direct injection operation are identified:

1. Poor low load performance at very high HES due to inadequate jet ignition by the reduced pilot.
2. Unstable combustion at low load as HES is increased due to delayed jet ignition by the reduced pilot.
3. Higher NO_x output compared to methane due to hydrogen's much faster burning rate, wider flammability limit and higher temperature combustion.
4. Further understanding of how various engine and injection parameters impact the flow field and combustion, emissions and performance characteristics is required.

The above issues will be investigated at multiple load conditions in a following study via exploration and optimisation of various parameters/approaches pertinent to 99% HES engine operation such as pilot injection timing, gaseous injection timing, number of injections, injector diameter, injection angle, EGR rate, turbocharging level and initial oxidiser charge temperature.

Declaration of competing interest

The authors declare that they have no known competing financial interests or personal relationships that could have appeared to influence the work reported in this paper.

REFERENCES

[1] IEA. Global Energy review 2021. Paris: IEA; 2021. Tech. Rep.
[2] Dicks AL, Rand DAJ. Fuel cell systems explained. John Wiley & Sons; 2018.
[3] Murugan A, Brown AS. Review of purity analysis methods for performing quality assurance of fuel cell hydrogen. Int J Hydrogen Energy 2015;40(11):4219–33. https://doi.org/10.1016/j.ijhydene.2015.01.041.
[4] Acar C, Dincer I. The potential role of hydrogen as a sustainable transportation fuel to combat global warming. Int J Hydrogen Energy 2020;45(5):3396–406. https://doi.org/10.1016/j.ijhydene.2018.10.149.
[5] Hosseini SE, Butler B. An overview of development and challenges in hydrogen powered vehicles. Int J Green Energy 2020;17(1):13–37. https://doi.org/10.1080/15435075.2019.1685999.
[6] Heywood J. Internal combustion engine fundamentals. McGraw-Hill Education; 1988.

Please cite this article as: Ramsay CJ, Dinesh KKJR, Numerical modelling of a heavy-duty diesel-hydrogen dual-fuel engine with late high pressure hydrogen direct injection and diesel pilot, International Journal of Hydrogen Energy, https://doi.org/10.1016/j.ijhydene.2023.09.019

[7] Dimitriou P, Tsujimura T. A review of hydrogen as a compression ignition engine fuel. Int J Hydrogen Energy 2017;42(38):24470–86. https://doi.org/10.1016/j.ijhydene.2017.07.232.
[8] Yip HL, Srna A, Yuen ACY, Kook S, Taylor RA, Yeoh GH, Medwell PR, Chan QN. A review of hydrogen direct injection for internal combustion engines: towards carbon-free combustion. Appl Sci 2019;9(22):4842. https://doi.org/10.3390/app9224842.
[9] Munshi S, Garner G, Theissl H, Hofer F, Razer B. Total cost of ownership (TCO) analysis for heavy duty hydrogen fueled powertrains, Tech. rep., Westport Fuel Systems and AVL List GmbH (1-10, February 25, 2021).
[10] Mohammadi A, Shioji M, Nakai Y, Ishikura W, Tabo E. Performance and combustion characteristics of a direct injection SI hydrogen engine. Int J Hydrogen Energy 2007;32(2):296–304. https://doi.org/10.1016/j.ijhydene.2006.06.005.
[11] Rottengruber H, Berckmüller M, Elsässer G, Brehm N, Schwarz C. Direct-injection hydrogen SI-engine - operation strategy and power density potentials, SAE Technical paper 2004-01-2927. Warrendale, PA: SAE International; Oct. 2004. https://doi.org/10.4271/2004-01-2927.
[12] Kim YY, Lee JT, Choi GH. An investigation on the causes of cycle variation in direct injection hydrogen fueled engines. Int J Hydrogen Energy 2005;30(1):69–76. https://doi.org/10.1016/j.ijhydene.2004.03.041.
[13] Tsujimura T, Suzuki Y. Development of a large-sized direct injection hydrogen engine for a stationary power generator. Int J Hydrogen Energy 2019;44(22):11355–69. https://doi.org/10.1016/j.ijhydene.2018.09.178.
[14] Li Y, Gao W, Zhang P, Ye Y, Wei Z. Effects study of injection strategies on hydrogen-air formation and performance of hydrogen direct injection internal combustion engine. Int J Hydrogen Energy 2019;44(47):26000–11. https://doi.org/10.1016/j.ijhydene.2019.08.055.
[15] Boretti AA, Watson HC. The lean burn direct injection jet ignition gas engine. Int J Hydrogen Energy 2009;34(18):7835–41. https://doi.org/10.1016/j.ijhydene.2009.07.022.
[16] Welch AB, Wallace JS. Performance characteristics of a hydrogen-fueled diesel engine with ignition assist. Warrendale, PA: SAE Technical Paper 902070, SAE International; Oct. 1990. https://doi.org/10.4271/902070.
[17] Homan HS, Reynolds RK, De Boer PCT, McLean WJ. Hydrogen-fueled diesel engine without timed ignition. Int J Hydrogen Energy 1979;4(4):315–25. https://doi.org/10.1016/0360-3199(79)90006-5.
[18] Furuhama S, Kobayashi Y. Development of a hot-surface-ignition hydrogen injection two-stroke engine. Int J Hydrogen Energy 1984;9(3):205–13. https://doi.org/10.1016/0360-3199(84)90120-4.
[19] Rosati MF, Aleiferis PG. Hydrogen SI and HCCI combustion in a direct-injection optical engine. SAE International Journal of Engines 2009;2(2009–01-1921):1710–36. https://doi.org/10.4271/2009-01-1921.
[20] Aleiferis PG, Rosati MF. Controlled autoignition of hydrogen in a direct-injection optical engine. Combust Flame 2012;159(7):2500–15. https://doi.org/10.1016/j.combustflame.2012.02.021.
[21] Gomes Antunes JM, Mikalsen R, Roskilly AP. An investigation of hydrogen-fuelled HCCI engine performance and operation. Int J Hydrogen Energy 2008;33(20):5823–8. https://doi.org/10.1016/j.ijhydene.2008.07.121.
[22] Gowda BD, Echekki T. Complex injection strategies for hydrogen-fueled HCCI engines. Fuel 2012;97:418–27. https://doi.org/10.1016/j.fuel.2012.01.060.
[23] Rottengruber H, Wiebicke U, Woschni G, Zeilinger K. Wasserstoff-Dieselmotor mit Direkteinspritzung, hoher Leistungsdichte und geringer Abgasemission. MTZ Mot Z 2000;61(2):122–8. https://doi.org/10.1007/BF03226557.
[24] Gomes Antunes JM, Mikalsen R, Roskilly AP. An experimental study of a direct injection compression ignition hydrogen engine. Int J Hydrogen Energy 2009;34(15):6516–22. https://doi.org/10.1016/j.ijhydene.2009.05.142.
[25] Babayev R, Andersson A, Dalmau AS, Im HG, Johansson B. Computational characterization of hydrogen direct injection and nonpremixed combustion in a compression-ignition engine. Int J Hydrogen Energy 2021;46(35):18678–96. https://doi.org/10.1016/j.ijhydene.2021.02.223.
[26] Babayev R, Andersson A, Serra Dalmau A, Im HG, Johansson B. Computational comparison of the conventional diesel and hydrogen direct-injection compression-ignition combustion engines. Fuel 2022;307:121909. https://doi.org/10.1016/j.fuel.2021.121909.
[27] Babayev R, Andersson A, Serra Dalmau A, Im HG, Johansson B. Computational optimization of a hydrogen direct-injection compression-ignition engine for jet mixing dominated nonpremixed combustion. Int J Engine Res 2022;23(5):754–68. https://doi.org/10.1177/14680874211053556.
[28] Frankl S, Gleis S, Karmann S, Prager M, Wachtmeister G. Investigation of ammonia and hydrogen as CO2-free fuels for heavy duty engines using a high pressure dual fuel combustion process. Int J Engine Res 2021;22(10):3196–208. https://doi.org/10.1177/1468087420967873.
[29] Liu X, Aljabri H, Panthi N, AlRamadan AS, Cenker E, Alshammari AT, Magnotti G, Im HG. Computational study of hydrogen engine combustion strategies: dual-Fuel compression ignition with Port- and Direct-Injection, Pre-Chamber Combustion, and Spark-Ignition. Fuel 2023;350:128801. https://doi.org/10.1016/j.fuel.2023.128801.
[30] Liu X, Seberry G, Kook S, Chan QN, Hawkes ER. Direct injection of hydrogen main fuel and diesel pilot fuel in a retrofitted single-cylinder compression ignition engine. Int J Hydrogen Energy 2022;47(84):35864–76. https://doi.org/10.1016/j.ijhydene.2022.08.149.
[31] Rorimpandey P, Yip HL, Srna A, Zhai G, Wehrfritz A, Kook S, Hawkes ER, Chan QN. Hydrogen-diesel dual-fuel direct-injection (H2DDI) combustion under compression-ignition engine conditions. Int J Hydrogen Energy 2023;48(2):766–83. https://doi.org/10.1016/j.ijhydene.2022.09.241.
[32] McTaggart-Cowan GP, Jones HL, Rogak SN, Bushe WK, Hill PG, Munshi SR. The effects of high-pressure injection on a compression-ignition, direct injection of natural gas engine. In: ASME 2005 internal combustion engine division fall technical conference. American Society of Mechanical Engineers Digital Collection; 2008. p. 161–73. https://doi.org/10.1115/ICEF2005-1213.
[33] Barba C, Dyckmans J, Förster J, Schnekenburger T. Natural gas-Diesel dual fuel for commercial vehicle engines. In: Liebl J, Beidl C, editors. Internationaler motorenkongress 2017, proceedings. Wiesbaden: Springer Fachmedien; 2017. p. 391–407. https://doi.org/10.1007/978-3-658-17109-4_23.
[34] Dai LM. Study of the injection and mixture process and the combustion simulation of natural gas/diesel dual-fuel, masters dissertation. Zhenjiang, China: Jiangsu University; 2016.
[35] Mabson CWJ. Emissions characterization of paired gaseous jets in a pilot-ignited natural-gas compression-ignition engine. Vancouver: MSc, The University of British Columbia; 2015.
[36] Kheirkhah P. CFD modelling of injection strategies in a high-pressure direct-injection (HPDI) natural gas engine. Vancouver: MSc, The University of British Columbia; 2015.
[37] Rochussen J, McTaggart-Cowan G, Kirchen P. Parametric study of pilot-ignited direct-injection natural gas

Please cite this article as: Ramsay CJ, Dinesh KKJR, Numerical modelling of a heavy-duty diesel-hydrogen dual-fuel engine with late high pressure hydrogen direct injection and diesel pilot, International Journal of Hydrogen Energy, https://doi.org/10.1016/j.ijhydene.2023.09.019

combustion in an optically accessible heavy-duty engine. Int J Engine Res 2020;21(3):497–513. https://doi.org/10.1177/1468087419836877.
[38] Jud M, Wieland C, Fink G, Sattelmayer T. Numerical analysis of the combustion process in dual-fuel engines with direct injection of natural gas. In: ASME 2018 internal combustion engine division fall technical conference. American Society of Mechanical Engineers Digital Collection; 2019. https://doi.org/10.1115/ICEF2018-9579.
[39] Faghani E. Effect of injection strategies on particulate matter emissions from HPDI natural-gas engines. Vancouver: Ph.D. thesis, The University of British Columbia; 2015.
[40] Chaichan M. The impact of equivalence ratio on performance and emissions of a hydrogen-diesel dual fuel engine with cooled exhaust gas recirculation. Int J Sci Eng Res 2015;6:938–41.
[41] van Lipzig JPJ, Nilsson EJK, de Goey LPH, Konnov AA. Laminar burning velocities of n-heptane, iso-octane, ethanol and their binary and tertiary mixtures. Fuel 2011;90(8):2773–81. https://doi.org/10.1016/j.fuel.2011.04.029.
[42] Haynes WM. CRC handbook of chemistry and physics. 95th ed. CRC Press; 2014.
[43] Alternative fuels data center. https://www.afdc.energy.gov/fuels/fuel_properties.php. [Accessed June 2018].
[44] Turns SR. An introduction to combustion: concepts and applications. 3rd ed. New York: McGraw-Hill Education; 2011.
[45] Green DW, Perry RH. Perry's chemical engineers' handbook. 8th ed. McGraw-Hill Education; 2008.
[46] Imhoff TB, Gkantonas S, Mastorakos E. Analysing the performance of ammonia powertrains in the marine environment. Energies 2021;14(21):7447. https://doi.org/10.3390/en14217447.
[47] Takizawa K, Igarashi N, Takagi S, Tokuhashi K, Kondo S. Quenching distance measurement of highly to mildly flammable compounds. Fire Saf J 2015;71:58–68. https://doi.org/10.1016/j.firesaf.2014.11.013.
[48] Zeldovich YB. Selected works of yakov borisovich zeldovich ch 26. Oxidation of nitrogen in combustion and explosions". of Selected Works of Yakov Borisovich Zeldovich, Princeton University Press 2014;1.
[49] Fenimore CP. Formation of nitric oxide in premixed hydrocarbon flames. Symposium (International) on Combustion 1971;13(1):373–80. https://doi.org/10.1016/S0082-0784(71)80040-1.
[50] Brookes SJ, Moss JB. Predictions of soot and thermal radiation properties in confined turbulent jet diffusion flames. Combust Flame 1999;116(4):486–503. https://doi.org/10.1016/S0010-2180(98)00056-X.
[51] C. J. Ramsay, K. K. J. R. Dinesh, High pressure direct injection of gaseous fuels using a discrete phase methodology for engine simulations, Int J Hydrogen Energy doi:10.1016/j.ijhydene.2021.10.235.
[52] Hessel RP, Abani N, Aceves SM, Flowers DL. Gaseous fuel injection modeling using a gaseous sphere injection methodology, SAE Technical paper 2006-01-3265. Warrendale, PA: SAE International; Oct. 2006. https://doi.org/10.4271/2006-01-3265.
[53] J. C. Beale, R. D. Reitz, Modeling spray atomization with the kelvin-helmholtz/Rayleigh-Taylor hybrid model, Atomization Sprays 9 (6). doi:10.1615/AtomizSpr.v9.i6.40.
[54] O'Rourke PJ. Collective drop effects on vaporizing liquid sprays, Tech. Rep. LA-9069-T. NM (USA: Los Alamos National Lab.; Nov. 1981.
[55] Liu AB, Mather D, Reitz RD. Modeling the effects of drop drag and breakup on fuel sprays. SAE Trans 1993;102:83–95. arXiv:44611358.
[56] O'Rourke PJ, Amsden AA. A spray/wall interaction submodel for the KIVA-3 wall film model. SAE Trans 2000;109:281–98. arXiv:44634219.
[57] Stanton DW, Rutland CJ. Modeling fuel film formation and wall interaction in diesel engines. SAE Trans 1996;105:808–24. arXiv:44736319.
[58] Gosman AD, loannides E. Aspects of computer simulation of liquid-fueled combustors. J Energy 1983;7(6):482–90. https://doi.org/10.2514/3.62687.
[59] Shih T-H, Liou WW, Shabbir A, Yang Z, Zhu J. A new k-epsilon eddy viscosity model for high Reynolds number turbulent flows. Comput Fluid 1995;24(3):227–38. https://doi.org/10.1016/0045-7930(94)00032-T.
[60] Pope SB. Computationally efficient implementation of combustion chemistry using in situ adaptive tabulation. Combust Theor Model 1997;1(1):41–63. https://doi.org/10.1080/713665229.
[61] Nordin N. Numerical simulations of non-steady spray combustion using a detailed chemistry approach. Licentiate of Engineering, Chalmers University of Technology, Dept. of Thermo and Fluid Dynamics; 1998.
[62] Smith G, Golden D, Frenklach M, Moriarty N, Eiteneer B, Goldenberg M, Bowman C, Hanson R, Song S, Gardiner W, Lissianski VV, Qin Z. GRI-Mech 3.0. http://www.me.berkley.edu/gri_mech/.
[63] Kéromnès A, Metcalfe WK, Heufer KA, Donohoe N, Das AK, Sung C-J, Herzler J, Naumann C, Griebel P, Mathieu O, Krejci MC, Petersen EL, Pitz WJ, Curran HJ. An experimental and detailed chemical kinetic modeling study of hydrogen and syngas mixture oxidation at elevated pressures. Combust Flame 2013;160(6):995–1011. https://doi.org/10.1016/j.combustflame.2013.01.001.
[64] Pomraning E, Richards K, Senecal PK. Modeling turbulent combustion using a RANS model, detailed chemistry, and adaptive mesh refinement, SAE Technical paper 2014-01-1116. Warrendale, PA: SAE International; Apr. 2014. https://doi.org/10.4271/2014-01-1116.
[65] Senecal PK, Richards KJ, Pomraning E, Yang T, Dai MZ, McDavid RM, Patterson MA, Hou S, Shethaji T. A new parallel cut-cell cartesian CFD code for rapid grid generation applied to in-cylinder diesel engine simulations, SAE Technical paper 2007-01-0159. Warrendale, PA: SAE International; Apr. 2007. https://doi.org/10.4271/2007-01-0159.
[66] Z. Wang, K. K. Srinivasan, S. R. Krishnan, S. Som, A computational investigation of diesel and biodiesel combustion and NOx formation in a light-duty compression ignition engine, Combustion Institute (GO8602569). doi:https://www.osti.gov/biblio/1079596.
[67] Wijeyakulasuriya S, Jupudi RS, Givler S, Primus RJ, Klingbeil AE, Raju M, Raman A. Multidimensional modeling and validation of dual-fuel combustion in a large bore medium speed diesel engine. In: ASME 2015 internal combustion engine division fall technical conference. American Society of Mechanical Engineers Digital Collection; 2016. https://doi.org/10.1115/ICEF2015-1077.
[68] Hogg T, Stojanovic S, Tebbs A, Samuel S, Durodola J. A benchmark study on the flow metering systems for the characterisation of fuel injectors for future heavy duty commercial vehicles. Measurement 2020;153:107414. https://doi.org/10.1016/j.measurement.2019.107414.

Please cite this article as: Ramsay CJ, Dinesh KKJR, Numerical modelling of a heavy-duty diesel-hydrogen dual-fuel engine with late high pressure hydrogen direct injection and diesel pilot, International Journal of Hydrogen Energy, https://doi.org/10.1016/j.ijhydene.2023.09.019